Neurobiology of Disease xxx (2014) xxx–xxx

Contents lists available at ScienceDirect

Neurobiology of Disease

journal homepage: www.elsevier.com/locate/ynbdi

A novel neuroferritinopathy mouse model (*FTL* 498InsTC) shows progressive brain iron dysregulation, morphological signs of early neurodegeneration and motor coordination deficits

Federica Maccarinelli [a,1], Antonella Pagani [b,1], Anna Cozzi [b,c], Franca Codazzi [b], Giuseppina Di Giacomo [c], Sara Capoccia [d], Stefania Rapino [e], Dario Finazzi [a], Letterio Salvatore Politi [b], Francesca Cirulli [d], Marco Giorgio [e], Ottavio Cremona [b,c], Fabio Grohovaz [b,c,*,2], Sonia Levi [b,c,*,2]

[a] *Department of Molecular and Translational Medicine, University of Brescia, Italy*
[b] *San Raffaele Scientific Institute, Via Olgettina 60, 20132 Milano, Italy*
[c] *Vita-Salute San Raffaele University, Via Olgettina 58, 20132 Milano, Italy*
[d] *Section of Behavioral Neuroscience, Department of Cell Biology, Istituto Superiore di Sanità, Rome, Italy*
[e] *Department of Experimental Oncology, European Institute of Oncology, Via Adamello 16, 20139 Milan, Italy*

ARTICLE INFO

Article history:
Received 14 July 2014
Revised 1 October 2014
Accepted 29 October 2014
Available online xxxx

Keywords:
Neuroferritinopathy
Neurodegenerative disorder
Ferritin
Iron
Oxidative damage

ABSTRACT

Neuroferritinopathy is a rare genetic disease with a dominant autosomal transmission caused by mutations of the ferritin light chain gene (*FTL*). It belongs to Neurodegeneration with Brain Iron Accumulation, a group of disorders where iron dysregulation is tightly associated with neurodegeneration. We studied the 498–499InsTC mutation which causes the substitution of the last 9 amino acids and an elongation of extra 16 amino acids at the C-terminus of L-ferritin peptide. An analysis with cyclic voltammetry on the purified protein showed that this structural modification severely reduces the ability of the protein to store iron. In order to analyze the impact of the mutation *in vivo*, we generated mouse models for the some pathogenic human *FTL* gene in FVB and C57BL/6J strains.

Transgenic mice in the FVB background showed high accumulation of the mutated ferritin in brain where it correlated with increased iron deposition with age, as scored by magnetic resonance imaging. Notably, the accumulation of iron–ferritin bodies was accompanied by signs of oxidative damage. In the C57BL/6 background, both the expression of the mutant ferritin and the iron levels were lower than in the FVB strain. Nevertheless, also these mice showed oxidative alterations in the brain. Furthermore, post-natal hippocampal neurons obtained from these mice experienced a marked increased cell death in response to chronic iron overload and/or acute oxidative stress, in comparison to wild-type neurons. Ultrastructural analyses revealed an accumulation of lipofuscin granules associated with iron deposits, particularly enriched in the cerebellum and striatum of our transgenic mice. Finally, experimental subjects were tested throughout development and aging at 2-, 8- and 18-months for behavioral phenotype. Rotarod test revealed a progressive impaired motor coordination building up with age, *FTL* mutant old mice showing a shorter latency to fall from the apparatus, according to higher accumulation of iron aggregates in the striatum. Our data show that our 498–499InsTC mouse models recapitulate early pathological and clinical traits of the human neuroferritinopathy, thus providing a valuable model for the study of the disease. Finally, we propose a mechanistic model of lipofuscine formation that can account for the etiopathogenesis of human neuroferritinopathy.

Introduction

Iron dyshomeostasis is often associated with neurodegenerative diseases (Rouault, 2013; Vidal et al., 2008), however whether it is a primary cause of the neurodegenerative process or a secondary effect is still debated (Levi and Finazzi, 2014). An opportunity to investigate the iron involvement in neurodegenerative processes is the group of diseases, referred to as "Neurodegeneration with Brain Iron Accumulation"

Abbreviations: NF, neuroferritinopathy; *FTL*, ferritin light chain gene; FtL, ferritin light chain protein; FtH, ferritin heavy chain protein; Tg, transgenic; WT, wild type; ROS, reactive oxygen species.

* Corresponding authors at: Vita-Salute San Raffaele University, and San Raffaele Scientific Institute, Via Olgettina 58, 20132 Milano, Italy. Fax: +39 02 26434844.
E-mail addresses: grohovaz.fabio@hsr.it (F. Grohovaz), levi.sonia@hsr.it (S. Levi).

Available online on ScienceDirect (www.sciencedirect.com).

[1] The authors contributed equally to this work.
[2] The authors share senior authorship.

http://dx.doi.org/10.1016/j.nbd.2014.10.023
0969-9961/

(NBIA) (Dusek and Schneider, 2012), in which diagnostic imaging and autopsy findings reveal focal iron accumulation in specific regions of the brain. Neuroferritinopathy (NF) (or NBIA3, OMIM, 606159) belongs to this group of diseases. It is classified as an adult-onset extrapyramidal disorder, in which motor symptoms prevail, while cognitive decline is uncommon or very mild. NF is a rare autosomal dominant disease caused by mutations in exons 3 and 4 of the ferritin light chain (*FTL*) gene (Curtis et al., 2001; Muhoberac and Vidal, 2013).

Ferritin is an iron storage protein able to detoxify cells from the redox-active free iron, that exists in a prevalent cytosolic form and in a minor mitochondrial one (Arosio and Levi, 2010). The cytosolic ferritin is composed of 24 subunits that co-assemble in heteropolymers of H- and L-chains. The H chain has a ferroxidase activity that is necessary for ferric iron incorporation, while the L-chain assists and facilitates the nucleation of the ferric iron inside the cavity (Arosio and Levi, 2010). Until now, seven mutations responsible for NF were identified. Only one is a missense mutation in exon 3 of *FTL* found in a single subject (Maciel et al., 2005) and its causative role is dubious; all the other ones are nucleotide insertion that strongly modify the C-terminus of the L-chain (Curtis et al., 2001; Vidal et al., 2004; Mancuso et al., 2005; Devos et al., 2009; Ohta and Takiyama, 2012; Kubota et al., 2009; Nishida et al., 2014). The C-terminus is rich of inter-chain contacts connecting four subunits at the 4-fold symmetry axis that participate to protein assembly (Luscieti et al., 2010). It has been demonstrated that NF mutations reduce ferritin stability as well as its ability to retain iron within the cavity, and that they act in a dominant negative manner even when present in a low proportions, 2–3 subunits in the 24-mer shells (Luscieti et al., 2010; Cozzi et al., 2010). Actually, the nucleotide insertions/duplications alter the terminal part of the ferritin, the extent depending on the site of insertion. Notably, it was indicated that onset and severity of the disease correlate with the degree of alteration of the protein (Kubota et al., 2009). The mutants are ubiquitously expressed but the main pathological effects are observed in the brain and more specifically in the basal ganglia, where neurons seem to have a higher susceptibility. The 460InsA mutation was the first to be identified in a large number of families in West Anglia and, clinically, is the best characterized form of NF (Curtis et al., 2001). However, most of the experimental research on *in vitro* and animal models has been concentrated on the insertion of TC nucleotides in *FTL* gene (498–499InsTC mutation, analogous to the 497–498dupTC) that coding for a variant protein with the substitution of the last 9 amino acids and an extension of further 16 amino acids, which is biochemically more stable than the 460InsA mutant (Muhoberac and Vidal, 2013). These studies reported a reduction in the iron storage capacity of ferritin as well as the formation of ferritin aggregates, suggesting that these features might concur to the pathogenetic events of the disease (Baraibar et al., 2008). Other data support and extend these observations by providing evidence of oxidative damage in cells expressing two pathogenic L-ferritin variants in cell lines (460InsA and 498–499InsTC) (Cozzi et al., 2010, 2006) and in fibroblasts derived from a NF patient with 498–499InsTC mutation (Barbeito et al., 2010).

The only animal model of the disorder produced so far is a transgenic mouse overexpressing the 498–499InsTC human ferritin mutant (Vidal et al., 2008). These mice were reported to show nuclear and cytoplasmic aggregates of ferritin throughout the CNS and in other organs, a progressive neurological phenotype, a decreased mobility and a reduced life expectancy as well as an increase in the amount of iron in brain, with altered levels of the iron-related proteins (Vidal et al., 2008). Analysis of brain tissues from these mice indicated an accumulation of oxidized DNA in the mitochondria but no significant damage to the nuclear DNA (Deng et al., 2010); moreover, oxidative stress markers such as protein carbonylation and lipid peroxidation were reported (Barbeito et al., 2009).

Here we report a comprehensive study of the 498–499InsTC human ferritin mutants that includes: i) an electrochemical analysis of the recombinant mutated ferritin heteropolymer, which precisely defines functional alterations of the protein expressed in our mutant mice; ii) a thorough characterization of our transgenic model, which re-evaluates and extends biochemical, morphological and physiological defects; iii) a behavioral investigation of these mice, which formerly proves the pathologic effect of the expression of the mutated ferritin in aged subjects. Overall, our data further extend and redefine the knowledge of the effects exerted by mutated ferritin on cellular iron handling and, more specifically, on the neuronal susceptibility to oxidative stress and motor coordination deficit.

Material and methods

Generation of FTL-498InsTC transgenic mice

The human *FTL* cDNA bearing the 498–499InsTC mutation (Cozzi et al., 2006) was subcloned into the BamH1–XbaI site between the PGK promoter and the SV40 poly-adenylation signal of the pCCL.sin.cPPT.hPGK vector (Follenzi et al., 2000). The correct assembly of the construct was firstly verified by restriction mapping and then confirmed by DNA sequencing (data not shown). The transgene was excised from the vector by SfiI-HpaI restriction digestion and purified by gel extraction with the QIAEX II Gel Extraction Kit (Qiagen, Hilden, Germany) Transgenic mice were generated by pronuclear microinjection of the linearized fragment (shown in Fig. 1S panel A) into fertilized mouse eggs from the FVB/N mouse strain. Microinjection and egg implantation procedures were carried out at the Core Facility for Conditional Mutagenesis (CFCM) Unit at the San Raffaele Scientific Institute, Milano, Italy. Screening for the correct insertion of the transgene was carried out by PCR amplification of the *FTL1* gene. To this purpose, tail DNA was purified from offsprings of matings of the heterozygous founders with wild-type mice and amplified with the following combination of primers which were specifically designed to amplify a fragment of the human *FTL1* cDNA: forward primer (5′-GTCTCCTGAAGATGCAAAAC CAG-3′) and reverse primer (5′-AACCTCCACAGGCTGGGT-3′). The amplification product for construct insertion was of 275 bps (Fig. 1S B). One independent line of the *FTL*-498InsTC FVB mice was chosen for stable expression of the transgene, as assayed by Western blotting of the non-denaturated protein with the anti-human FtL mouse monoclonal-Ab (LF03, not shown). This *FTL*-498InsTC line was backcrossed with C57BL/6J (C57) mice (purchased from Harlan Laboratories Srl, Udine, Italy) for >6 generations for generating mice suitable for behavioral studies.

Transgenic mice were bred and housed under a 12 h light–dark cycle with free access to food and water.

Tissue preparations

Biochemical analysis was performed on FVB strain at different ages: 3, 6, 12, 18, 22 months-old. For each age were analyzed WT (n = 2 male and 1 female) and Tg (n = 2 male and 1 female). C57 mice were tested at 6,12,18 months-old (n = 2 male and 2 female) and Tg (n = 2 male and 2 female).

Mice were anesthetized with Avertine (23 μl/g mouse; Sigma) and perfused with a physiological saline solution containing 2% heparin; tissue samples were then removed and: i) immediately frozen for biochemical analysis; ii) immersed in PBS containing 4% paraformaldehyde 18 h for *ex vivo* MRI, immunofluorescence and Prussian Blue staining; iii) or immersed in PBS containing 4% paraformaldehyde and 2.5% glutaraldehyde for electron microscopy.

For biochemical analysis tissues were lysed in ice-cold lysis buffer (20 mM Tris buffer, pH 7.4, 1% Triton X-100, 1 mM Na azide, 1 mM PMSF, 10 mM leupeptin, 1 mM pepstatin) using a Potter homogenizer. The homogenate was clarified by centrifugation at 10,000 *g* for 10 min

Please cite this article as: Maccarinelli, F., et al., A novel neuroferritinopathy mouse model (*FTL* 498InsTC) shows progressive brain iron..., Neurobiol. Dis. (2014), http://dx.doi.org/10.1016/j.nbd.2014.10.023

at 4 °C, and the supernatant was used in Western blotting or in ELISA experiments.

For histochemistry and immunofluorescence experiments brains were incubated in PBS containing 4% of paraformaldehyde for 18 h, then, were washed with PBS and included in agarose (4% in PBS) for sectioning. Coronal slices of 40 μm were done with a Cryostate and, then, cryopreserved in a solution composed of 30% glycol ethylene, 30% glycerol and 40% PBS at −20 °C.

For electron microscopy analysis small pieces of fixed brains were dehydrated and embedded in Epon 812. Sections were cut with a diamond knife by an Ultracut UCT (Leica Microsystem, Wetzlar, Germany) and double stained with uranyl acetate and lead citrate

Ferritin quantification and protein immunodetection

Transgenic human ferritin levels were determined on Architect equipment of Abbot with reagents for the immunological determination of serum ferritin. We verified that the ELISA assay is specific for human L ferritin with no cross reaction with mouse ferritins. Endogenous L- and H-ferritins were quantified by ELISA using specific rabbit polyclonals antibodies, E17 and Z17 respectively calibrated on the corresponding recombinant homopolymer (Santambrogio et al., 2000). Protein concentration was evaluated by the bicinchoninic acid (BCA) method (Pierce) calibrated on BSA. The expression of the transgene was also confirmed by western blotting. 20 μg of soluble proteins were heated at 70 °C for 10 min, centrifuged at 13,000 rpm at 4 °C and the supernatants were separated by non-denaturing-PAGE (native-PAGE). Immunoblotting was performed using a specific antibody for human L ferritin (mouse monoclonal LF03) (Cozzi et al., 2006). To study iron incorporation capacity, equal amounts of the 70 °C heated samples were separated on native-PAGE and then the gels were stained with Prussian Blue and enhanced with 0.025% 3,3′-diaminobenzidine (DAB) and 0.05% H_2O_2 for 15 min. The expression of other proteins was assayed by analyzing 20 μg of homogenate soluble proteins separated by sodium dodecyl sulfate -PAGE (SDS-PAGE) and immunoblotting was performed using specific antibodies for Catalase (EMD, Millipore), TfR1 (Zymed), Ubiquitin (Santa Cruz Biotechnology) and β-actin (Sigma), followed by peroxidase-labeled secondary antibodies (Sigma-Aldrich). Band intensity was revealed by enhanced chemiluminescence (ECL; GE Healthcare).

Detection of protein, lipid and DNA oxidation

The following kits were used according to manufacturer's instructions:

- Oxidized proteins were revealed by the Oxyblot Protein Oxidation Detection Kit (EMD Millipore). In brief, the soluble protein extracts were derivatized to 2,4-dinitrophenylhydrazone (DNP), and 1 μg was loaded on 12% SDS-PAGE, blotted and incubated with an anti-DNP antibody, followed by an HRP conjugated secondary antibody. The bound activity was revealed by ECL advance (GE Healthcare).
- Lipid peroxidation was revealed by the OxiSelect MDA Immunoblot Kit (Cell Biolabs, Inc). In brief, 10 μg of the soluble protein extracts was loaded on 12% SDS-PAGE, blotted and incubated with an anti-MDA antibody and then with an anti-Rabbit IgG , HRP conjugate. The bound activity was revealed as above.
- Oxidative DNA damage, was detected in terms of 8-OHdG, by the OxiSelect Oxidative DNA Damage ELISA Kit (Cell Biolabs, Inc). Extract DNA from tissues treated with the nuclease P1 was used for competitive ELISA assay: the samples were first added to the 8-OHdG/BSA preabsorbed plates, then incubated with an anti-8-OHdG antibody, followed by an HRP conjugated secondary antibody. The absorbances were detected at 450 nm on a microplate reader.

Histochemistry

DAB-enhanced Prussian Blue staining was performed to identify iron deposition in serial 40 μm coronal mouse brain sections. Briefly, brain sections were washed twice with PBS, permeabilized with PBS/Triton 0.5% and then incubated for 1 h with 4% potassium ferrocyanide in 6% hydrochloric acid. Then slices were reacted with activated 0.014% DAB containing 0.03 H_2O_2 for 10 min and then washed three times with PBS. DAB staining was acquired with the Nuance Multispectral Tissue Imaging Systems (PerkinElmer) assembled on Zeiss Axioplan2 microscope and quantified with the Advanced Image Analysis Software inForm (PerkinElmer).

Immunofluorescence

Brain slices were washed twice in PBS and incubated with blocking solution (PBS with 10% FBS and 0,3% Triton X-100) for 1 h at room temperature. Then, tissues were incubated overnight at 4 °C with anti-ferritin primary antibody (LF03 5 μg/ml) diluted in blocking solution. Following 3 washes in PBS, cells were incubated with secondary antibody in PBS (donkey anti-mouse Alexa 488; Molecular Probes) for 90 min at room temperature. Tissues were also stained for NeuroTrace 530/615 (a neuronal marker, diluted 1:100 in PBS; Molecular Probes) and TO-PRO-3 (a nuclear marker diluted 1:1000 in PBS; Molecular Probes). All brain slices were mounted on glass slide using Fluorsave (Calbiochem) and acquired on confocal microscope (BioRad confocal).

Magnetic resonance imaging (MRI)

For *in vivo* MRI, mice were anesthetized with gas (2% Isoflurane in oxygen) and brain acquisitions were done with a 7 T MR scanner (Bruker Biospec 30/70, Ettlingen, Germany) and a 4 channel dedicated mouse brain phased-array coil.

2D Fast Low Angle SHot (FLASH) Susceptibility Weighted Imaging (SWI) images [repetition time (TR) = 474.5 ms; echo time (TE) = 15 ms; flip angle (FA) = 30°; number of excitations (NEX) = 10; field of view (FOV) = 2.5 cm; slice thickness/inter-slice distance = 0.6 mm; acquisition matrix = 512 × 384] and multiecho Rapid Acquisition with Relaxation Enhancement (RARE) T2 sequence (TR = 3851.8 ms; 16 echoes with TE ranging from 11 to 176 ms; NEX = 2; FOV = 2.5 cm; slice thickness/inter-slice distance = 0.6 mm; acquisition matrix = 198 × 198) were acquired. T2 maps were calculated using the manufacturer's software (Paravision 5.1). In order to evaluate the local relaxation times, circular ROIs of the same size ($4 * 10^5$ μm^2) over different areas of the brain (cortex, striatum, hippocampus, pons and cerebellum) were drawn by the same operator on T2 images and then transferred on T2 maps.

For *ex vivo* imaging, brain acquisitions were performed on a human grade 3 T MRI scanner (Achieva 3 T, Philips Medical Systems, the Netherland) equipped with a mouse dedicated volumetric coil. The following sequences were: 3D Turbo Spin Echo T2 (TR = 2500 ms; TE = 90 ms; Turbo Spin Echo Factor = 4; NEX = 4; FOV = 2.5 × 1.2 × 1.2 cm; slice thickness = 0.5 × 0.5 × 0.5 mm; acquisition matrix = 256 × 128) and SWI (TR = 61 ms; TE 40 ms; flip angle = 30°; NEX = 28; FOV = 3.5 × 1.9 × 1.4 cm; slice thickness = 0.1 mm; acquisition matrix = 336 × 184).

Electron spectroscopic imaging

The thin sections (~25 nm, gray tone) analyzed by Electron Spectroscopic Imaging (ESI) were first examined at 250 eV (*i.e.* at an energy loss where scattered electrons of most elements contribute to the image),

Please cite this article as: Maccarinelli, F., et al., A novel neuroferritinopathy mouse model (*FTL* 498InsTC) shows progressive brain iron..., Neurobiol. Dis. (2014), http://dx.doi.org/10.1016/j.nbd.2014.10.023

thus providing a general view of the ultrastructural organization (Pezzati et al., 1997). The pattern of net iron distribution was then obtained by computer-assisted processing of two images collected below (651 and 683 eV) and one beyond the Fe-L3 absorption edge at 719 eV. The typical energy width of the imaging electrons was −5 eV. A threshold of iron values was routinely set to exclude random noise from the final representation. The map thus obtained, represented according to a pseudocolor scale (from dark red to yellow), was superimposed to the corresponding 250-eV image. The nature of iron signals in the maps was confirmed by EELS spectra.

Autofluorescence spectra

Since lipofuscin is a native autofluorescent material we tested its possible presence by exposing brain sections to excitation at two wavelengths: 458 and 514 nm in a Leica SP2 confocal microscope. The lambda scan mode was selected and the detection window width was set to 10 nm. The PMT offset was left at 0. The detection window was moved to the different laser lines and the PMT gain adjusted so that the reflection image at each line was below saturation. AOTF settings for each laser line were adjusted to obtain similar peak intensities. The lambda scan was performed in 10 nm intervals (exc. 458, em. 480–700 nm; exc. 514, em. 540–740).

Recombinant ferritins

The recombinant human ferritin homopolymers and heteropolymers were produced in *Escherichia coli* as described in Luscieti et al., 2010. The heteropolymers were produced by a bicistronic expression vector in which the sequence of the Ferritin H chain was followed by a ribosome binding site and by the sequence of the L-chain, wild type or mutated. This construct produced in *E. coli* heteropolymers composed by 20–22 H chain and 4–2 L-chains, which are expected to mimic the subunit composition of the brain ferritin. The proteins were purified and loaded with 1000 Fe atoms per molecule before cyclic voltammetry studies. $FtL_{167fsx26}$ corresponds to the protein encoded by the 498–499InsTC mutation.

Cyclic voltammetry

Cyclic voltammetry investigations were performed to determine the electrochemical properties of recombinant ferritins (in Tris 30 mM pH 7.4) and accomplished using a CHI 210B bipotentiostat (CHI Instrument Inc., Texas, USA). All potentials are referred to Ag/AgCl reference electrode.

We used screen printed gold electrodes (DROPSENS, Llanera, Spain) designed for electrochemical investigation of small sample volumes in order to enable the direct characterization of the dissolved proteins. Using the aforementioned strategy, additional surface adsorption procedures were avoided, that could potentially interfere with the protein functioning and with the iron release/uptake kinetics (Bard and Faulkner, 2001)

Primary culture of hippocampal neurons

The hippocampal cultures were prepared from 1–2 d-old transgenic (Tg)-C57 and wild-type (WT)-C57 mice, according to Codazzi et al. (2006). Briefly, the hippocampal sections were digested into Hank's solution containing 3.5 mg/ml trypsin type IX (Sigma, St. Louis, MO) and 0.5 mg/ml DNase type IV (Calbiochem, La Jolla, CA) for 5 min and then mechanically dissociated in a Hank's solution supplemented with 12 mM Mg_2SO_4 and 0.5 mg/ml DNase IV. After centrifugation, the pool of the neurons obtained from control and transgenic mice were plated onto polyornithine-coated 96-multi wells and maintained in MEM supplemented with 0.3% glucose, B27 supplement, 2 mM glutamax, 5% fetal calf serum, and 3 μM Ara-C (1-D-cytosine-arabinofuranoside) (Sigma). Cultures were maintained at 37 °C in a 5%CO2 humidified incubator, and used from 1 to 2 weeks after plating.

Cell death analysis

Hippocampal neurons were maintained in culture for one to two weeks. Before the experiment, cells were washed with Krebs Ringer Hepes buffer (KRH, containing 5 mM KCl, 125 mM NaCl, 2 mM CaCl2, 1.2 mM MgSO4, 1.2 mM KH2PO4 and 6 mM glucose, 20 mM Hepes, pH 7.4). Cell death and vital analyses were performed by exposing the cells in Sytox Orange and Hoechst 33342, respectively (5 μM in KRH, 5 min incubation at room temperature). The analysis was performed by a High Throughput Microscopy (HTM) system, the IN Cell Analyzer 1000 (GE Healthcare, Grandview Blvd, Waukesha, WI, USA).

Behavioral test

Motor coordination and balance were tested using an accelerating rotarod (Accelerating Rotarod, Ugo Basile, Gemonio, Italy). The rotarod test was specifically designed for automated measurements of neurological deficits in rodents; it allows studying motor coordination using the natural fear of falling response in mice (Brooks and Dunnett, 2009). Latency to fall is a more stringent measure of ability to maintain balance, since the requirements for running forward are gradually increasing. Mice with deficits in motor coordination or balance fall off the rotarod before the end of the 5-minute test session (Crawley, 1999). Deficits in the rotarod test can be caused by pathology in the cortex, cerebellum, and spinal cord, in addition to pathology in dopaminergic regions such as the substantia nigra and striatum. More in detail, GABAergic interneurons in the dorsal striatum are seemingly crucial for facilitating fine movement, as GABAergic dysfunction in the striatum has been linked with hyperkinetic movements and motor coordination (Plenz and Kitai, 1998; Do et al., 2013).

Mice were tested at different ages: a) young mice, 2 months-old (n = 7 male and 7 female WT; n = 8 male and 8 female Tg); b) adult mice, 8 months-old (n = 18 male and 12 female WT; n = 15 male and 13 female Tg); c) aged mice, 18 months-old (n = 6 male and 5 female WT; n = 5 male and 5 female Tg). The test was performed by placing a mouse on a rotating rod with a diameter of 3 cm and measuring the latency to fall (in seconds), through a switch placed on the floor below. Mice were given three trials each with a maximum time of 300 s (5 min), during which time the rotating rod underwent a linear acceleration from 4 to 40 rpm over 5 min. Animals were rested a minimum of 10 min between trials to avoid fatigue and exhaustion (Paylor et al., 2006).

Statistical analyses

Data, except where otherwise indicated, are reported as the mean ± SD values or as a representative of at least three independent experiments with similar results. Statistically significant differences between CTR and Tg mice were determined by the Student's *t* test, at three different level $^{*}p \leq 0.05$; $^{**}p \leq 0.01$; $^{***}p \leq 0.001$.

Behavioral data were analyzed using parametric analysis of variance (ANOVA) with "genotype" (WT and Tg) and "gender" (male and female) as between-subjects factors and "trial" as within-subject repeated measure. Post hoc comparisons were performed by the Tukey's test. Statistical analysis was performed using Statview II (Abacus Concepts, CA, USA). Data are expressed as mean ± SEM. The level of significance was set at 0.05.

Experimental procedures and animal care approval

Animal handling and experimental procedures were performed in accordance with the EC guidelines (EC Council Directive 86/609 1987) and with the Italian legislation on animal experimentation

Please cite this article as: Maccarinelli, F., et al., A novel neuroferritinopathy mouse model (*FTL* 498InsTC) shows progressive brain iron..., Neurobiol. Dis. (2014), http://dx.doi.org/10.1016/j.nbd.2014.10.023

(Decreto L.vo 116/92). All the experiments performed at the San Raffaele Scientific Institute and at the University of Brescia were approved by the internal Institutional Animal Care and Use Committees (IACUC).

Results

Recombinant human mutant FtL (498–499InsTC) shows reduced capacity to incorporate iron

Our previous results, obtained with recombinant ferritin heteropolymer, suggested that the presence of a few mutant L-chain alters the permeability of ferritin and its capacity to retain iron (Luscieti et al., 2010). Since electron-transfer reactions are involved in the iron loading and unloading of ferritin (Ritzert et al., 2009), we explored the capacity of mutated ferritin to retain iron *in vitro*, by cyclic voltammetry. To this aim, we employed two recombinant heteropolymer ferritins constituted by H and L-chains: the FtH/FtL, which mimics the form present in normal brain and the FtH/Ft$L_{167Sfsx26}$, the variant form encoded by the 498–499InsTC mutation (Fig. 1A). These ferritins were used to investigate the kinetics and energies of iron release. We found that the energy of iron release is different for the FtH/Ft$L_{167Sfsx26}$: compared to the FtH/FtL form, the iron catalytic release of the mutant specie started at a lower potential (~25 mV; Fig. 1B). This implies that the iron release from the ferritins containing the mutant L-chain occurs under milder conditions with a consequent increased iron concentration in the proximity of the mutant protein. Moreover, the oxidation waves in the cyclic voltammograms show only one peak for the FtH/FtL, at 360 mV, and two different peaks for the FtH/Ft$L_{167Sfsx26}$, at 300 mV and 480 mV, respectively (Fig. 1B). These results suggest that also the oxidation/uptake iron route is modified by the mutation.

Finally, an electrochemical evaluation of the reactive oxygen species (ROS) production was performed in the presence of ferritins. Our data demonstrate that the FtH/Ft$L_{F167SfsX26}$ produces more effectively ROS species in physiological solutions compared to FtH/FtL. In these measurements, oxygen reduction is related to the generation of ROS. The graph (Fig. 1C) shows that the oxygen reduction current is 30% higher for FtH/Ft$L_{F167SfsX26}$ than for the FtH/FtL, proving that in the presence of the variant ferritin iron is less retained and ROS are more efficiently generated.

Generation of a murine model for the neuroferritinopathy human mutant FTL (498–499InsTC)

To produce an animal model for neuroferritinopathy, we generated transgenic mice by pronuclear microinjection in FVB mouse strain (the standard strain to produce transgenic mice) of the vector for the human mutant *FTL* gene (498–499InsTC). The expression of the transgene was driven by the constitutive and ubiquitous PGK promoter (Fig. 1S, A). The mice were genotyped by PCR using primers to specifically amplify a 275 bp fragment of the human *FTL* gene (arrows in Fig. 1S A and amplification band in B); no cross-amplification of the mouse *FTL* gene or pseudogenes can be detected in WT offsprings (Fig. 1S, B). Three transgenic lines were obtained and analyzed for transgene expression by RT-PCR. The transgene transcript was detected in all tissues analyzed, including brain and liver (not shown). Then, the expression of the transgenic protein was assessed by ELISA and by immunoblotting of non-denaturing PAGE with a monoclonal antibody specific for the assembled human FtL (LF03), that does not cross react with the endogenous mouse ferritins (Santambrogio, 2000). In 3-month-old mice, the expression of the transgene was high in the liver and even greater in the brain (Fig. 1S, B). Based on the protein expression levels, we selected one of the mouse lines for establishing the colony and for further studies. Transgenic (Tg-FVB) and control FVB (WT-FVB) mice were followed for up to two years.

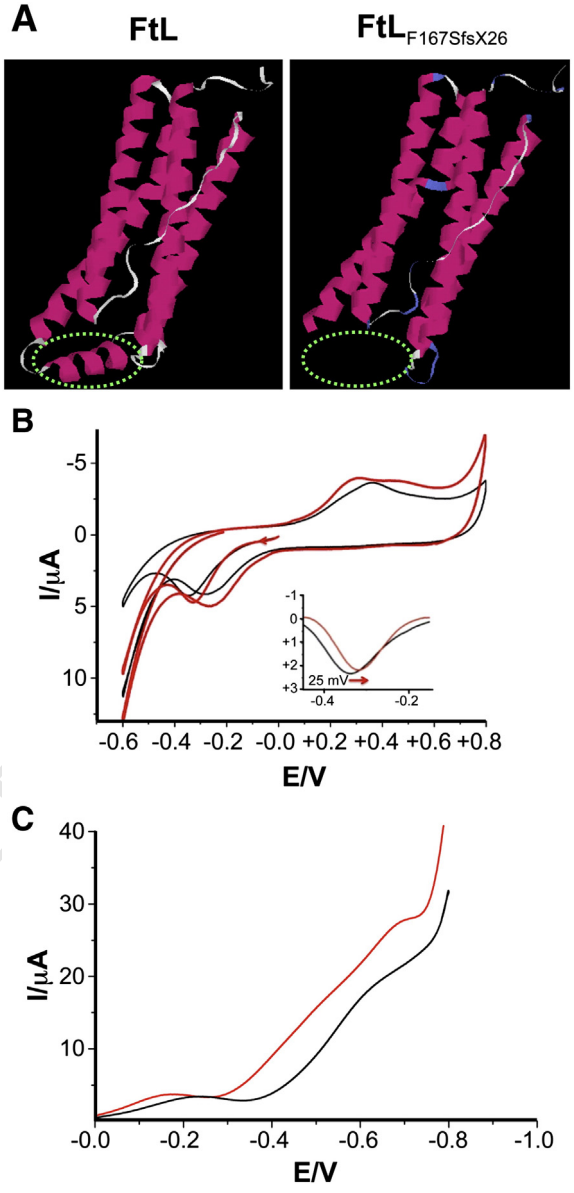

Fig. 1. Mutant Ft$L_{F167SfsX26}$ has a reduced capacity to incorporate iron. A 3D representation of L-ferritin subunit (FtL) and of its mutant (Ft$L_{F167SfsX26}$). Figures were drawn using the molecular graphics program PyMOL. The model highlights the loss of conformation of the E-helix (green dashed line) in the mutant protein, with consequent widening of the channel open to the inner cavity. B The cyclic voltammograms of FtH/Ft$L_{F167SfsX26}$ (red lines) and FtH/FtL protein (black lines) report the current signal (I/μA) measured as the electrode potential changes (E/V) linearly with 100 mV/s scan rate (see Material and methods). It shows that the iron catalytic release of Ft$L_{F167SfsX26}$ starts at a lower potential (~25 mV, see inset: the first forward scan background corrected is shown for the two species). C The graph shows the oxygen reduction currents vs. applied potentials: FtH/Ft$L_{F167SfsX26}$ produces an augmented reduction current with higher generation of ROS.

The brain of Tg-FVB mice shows increased expression of mutated human FTL and oxidative damage

Groups of three WT-FVB and Tg-FVB mice were sacrificed, the brains collected and the protein extracts analyzed by ELISA for the expression of human FtL as well as of the endogenous FtL and FtH at different ages (3, 6, 12 and ≥18 months). Accumulation of transgenic human FtL increased progressively with age and reached a maximum of about 4 μg/mg of total proteins at 18 months of age (Fig. 2A, upper panel). Also the accumulation of the soluble endogenous murine FtL and FtH increased with age, but they reached a maximum at 12 months. At this

Please cite this article as: Maccarinelli, F., et al., A novel neuroferritinopathy mouse model (*FTL* 498InsTC) shows progressive brain iron..., Neurobiol. Dis. (2014), http://dx.doi.org/10.1016/j.nbd.2014.10.023

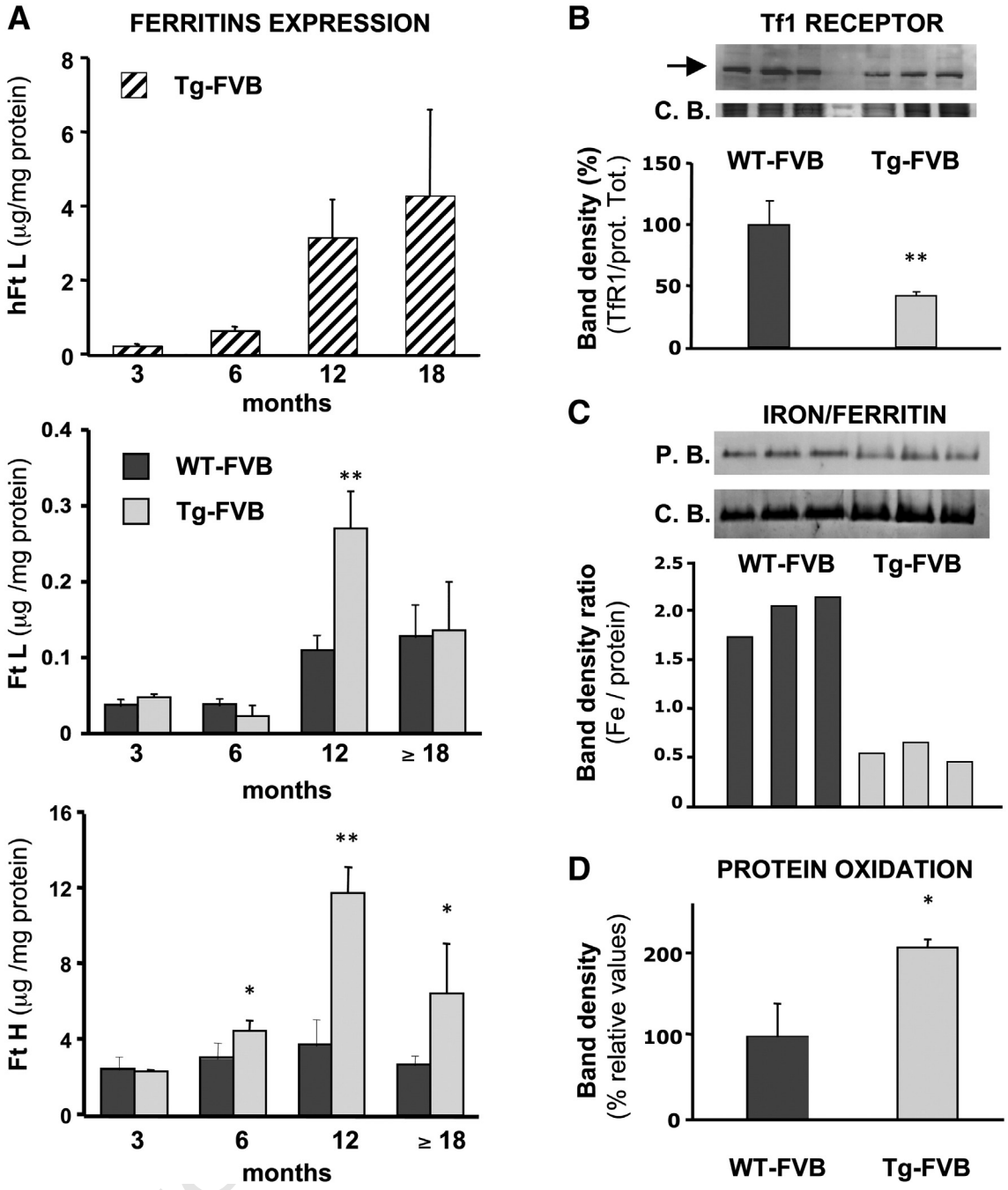

Fig. 2. Increased expression of mutated human *FTL* induces elevation of cytosolic iron and oxidative damage in Tg-FVB mice brains. A. The soluble brain homogenate fractions of WT-FVB and Tg-FVB mice at different ages were analyzed for human L-ferritin (*upper panel*) and endogenous L- and H-ferritins (*middle and bottom panel, respectively*) content by specific ELISA. The values are the means of three experiments performed in triplicate. B 20 µg of brain homogenates of 12-month-old mice were loaded on 12% SDS-PAGE and blotted with an anti TfR1 antibody (the arrow points to the TfR1). Coomassie blue staining (C.B.) of total protein as loading control. Band densities are reported in the lower panel. C Enhanced Prussian Blue (P.B.) staining of brain soluble homogenates of 12-month-old Tg-FVB mice and WT-FVB siblings (native-PAGE). Coomassie blue staining (C.B.) of ferritin protein as loading control. The histogram shows the iron incorporation capacity of the ferritin in the two groups of animals as the ratio between the total ferritin iron and the ferritin protein content in the same brain extract. D The carbonilated proteins of brain homogenate of 12-month-old WT-FVB and Tg-FVB were revealed by treating with DNPH and blotting with anti-DNP antibody as described in Material and methods. Band densities are expressed as values relative to the mean of the controls of three independent experiments $^{*}p \leq 0.05$.

time point, Tg-FVB brains showed 2.5 and 3.1 fold higher levels of FtL and FtH than WT-FVB, respectively (Fig. 2A, middle and lower panels). Immunoblotting analysis of the Transferrin Receptor 1 (TfR1) showed in the brain of Tg-FVB mice a significant reduction (~58%, $^{**}p \leq 0.001$; Fig. 2B) that was paralleled by that of mRNA level (~50% reduction, $^{*}p \leq 0.05$; obtained by qRT-PCR, not shown). The increase in endogenous ferritin and the concomitant decrease in TfR1 indicate the high availability of intracellular iron, a condition that is line with our experimental evidence that iron is not properly retained inside the cavity of variant ferritins.

We analyzed total ferritin iron and ferritin protein on the same brain extracts. This was done by staining non-denaturing PAGE with enhanced Prussian Blue and with Coomassie blue (Fig. 2C). The analysis of the band densities clearly indicates that the iron/protein ratio

Please cite this article as: Maccarinelli, F., et al., A novel neuroferritinopathy mouse model (*FTL* 498InsTC) shows progressive brain iron..., Neurobiol. Dis. (2014), http://dx.doi.org/10.1016/j.nbd.2014.10.023

(Fig. 2C) was lower in Tg-FVB than in WT-FVB mice, indicating a reduced capacity of the ferritin in the Tg mice to incorporate iron *in vivo*. Since this condition is expected to promote oxidative damage, we evaluated the oxidative status of brain tissues by OxyBlot. The transgenic mice showed a higher level of carbonylated proteins already at 6 months (not shown) and reached a two fold increase at 12 months (Fig. 2D, $^{*}p \leq 0.05$).

Tg-FVB mice show iron and ferritin accumulation in the brain

The pathologic hallmark of the human disease is the accumulation of iron and ferritin bodies in the brain and other tissues, with late onset neurological symptoms. Based on this premise, brain from old mice were investigated for iron and ferritin content. First, we evaluated iron accumulation in wild-type and transgenic mice *in vivo* by MRI. The MRI changes associated with iron deposition were investigated in Tg-FVB mice at 18 and 22 months of age as modification of the signal intensity in T2-weighted images (Fig. 3A, left panel, upper row) and in SWI images (Fig. 3A, left panel, lower row). In all Tg-FVB mice, an overall darker appearance could be observed at the level of the cortex and hippocampus in all sequences suggesting diffuse neuronal iron deposition. Further, several hypointense spots highly evocative of iron aggregation could be detected on SWI images in the striatum and Hippocampal cortex of 18 and 22 month-old Tg-FVB mice, but not in age-related WT mice. Using T2 relaxometry, *in vivo* MRI T2 maps were generated and showed a significant decrease in the T2 decay, a parameter that is well known to correlate with iron deposition, in the frontal cortex, striatum, hippocampus, pons and cerebellum of Tg-FVB mice (Fig. 3B, $^{*}p \leq 0.05$; $^{**}p \leq 0.01$; $^{***}p \leq 0.001$). As expected, these observations were corroborated by *ex vivo* MRI analyses which confirmed the presence of the above described hypointense areas on high resolution 3D T2 and SWI sequences (Fig. 3A, right panel). These data most likely indicate the increased level of iron in the brain of living mice expressing mutant *FTL*.

To verify that iron accumulates in mutant brains, we performed histochemical analysis of iron by DAB-enhanced prussian blue stain. DAB-stained sections of 18 and 22 month-old mutant brains showed a large increase in the number of brown positive precipitates over control mice, with no significant variations between the two ages (Fig. 4A). This result indicates iron accumulation when the human transgene is expressed.

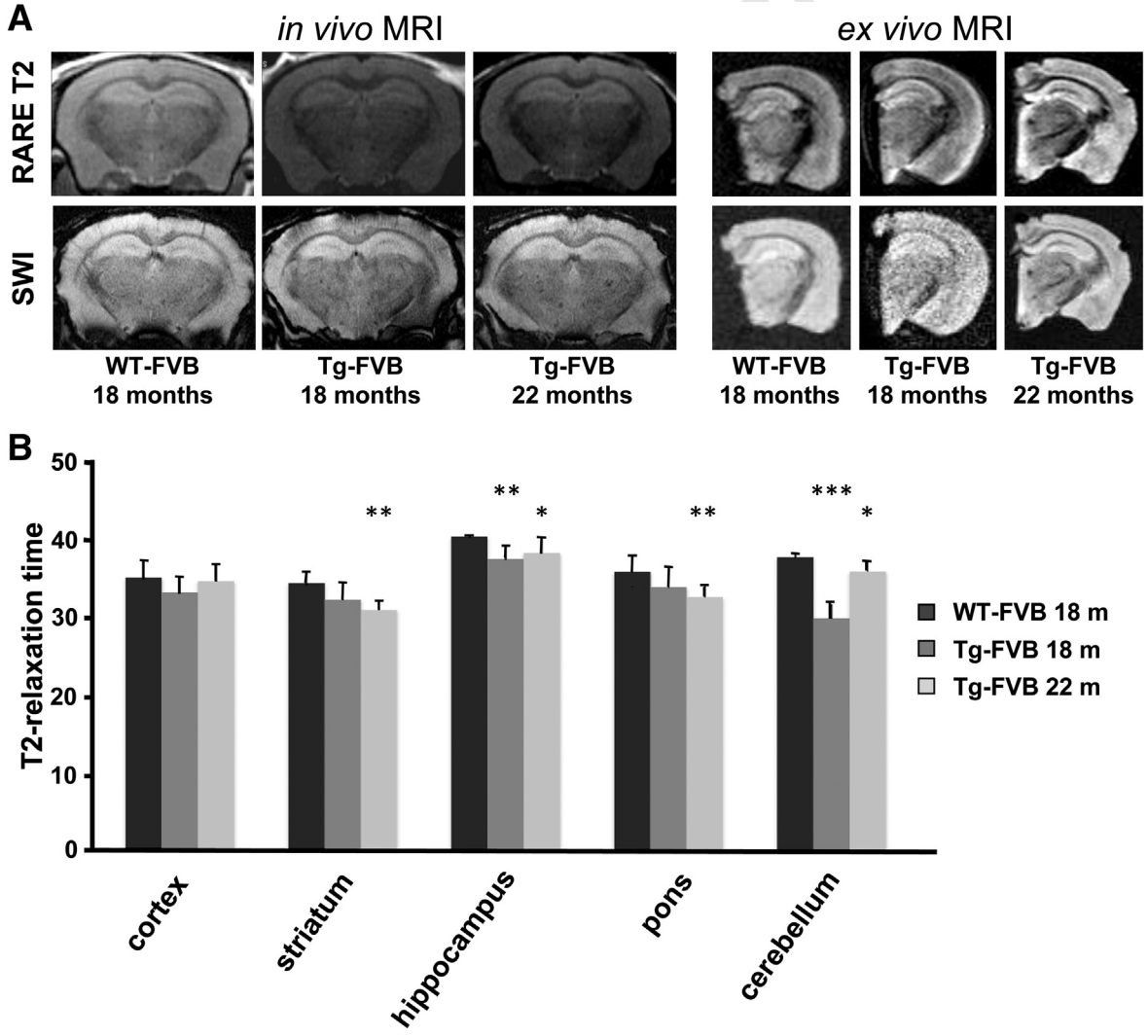

Fig. 3. Iron accumulation in whole brain of FVB mutated mice. A MRI brain examination of 18 and 22 month-old controls and transgenic FVB mice. *Left panel*: RARE T2 (*upper row*) and SWI (*lower row*) coronal images are shown. Areas of brain iron accumulation are detected *in vivo* as multiple small dark hypointense areas. *Right panel*: the brain from the same animals were analyzed *ex vivo*, Fast Spin Echo T2 (*upper row*) and SWI (*lower row*) images confirm the results obtained *in vivo* and show the presence of iron accumulation at the level of the hippocampus, brain cortex and basal ganglia. B *In vivo* T2 relaxation times of WT- and Tg-FVB mice at 18 and 22 months of age measured on T2 maps. These measurements revealed a significant reduction of the T2 decay in the brains of Tg mice with respect to the control, in particular in striatum, hippocampus, cerebellum and pons, highly suggestive of iron accumulation.

Please cite this article as: Maccarinelli, F., et al., A novel neuroferritinopathy mouse model (*FTL* 498InsTC) shows progressive brain iron..., Neurobiol. Dis. (2014), http://dx.doi.org/10.1016/j.nbd.2014.10.023

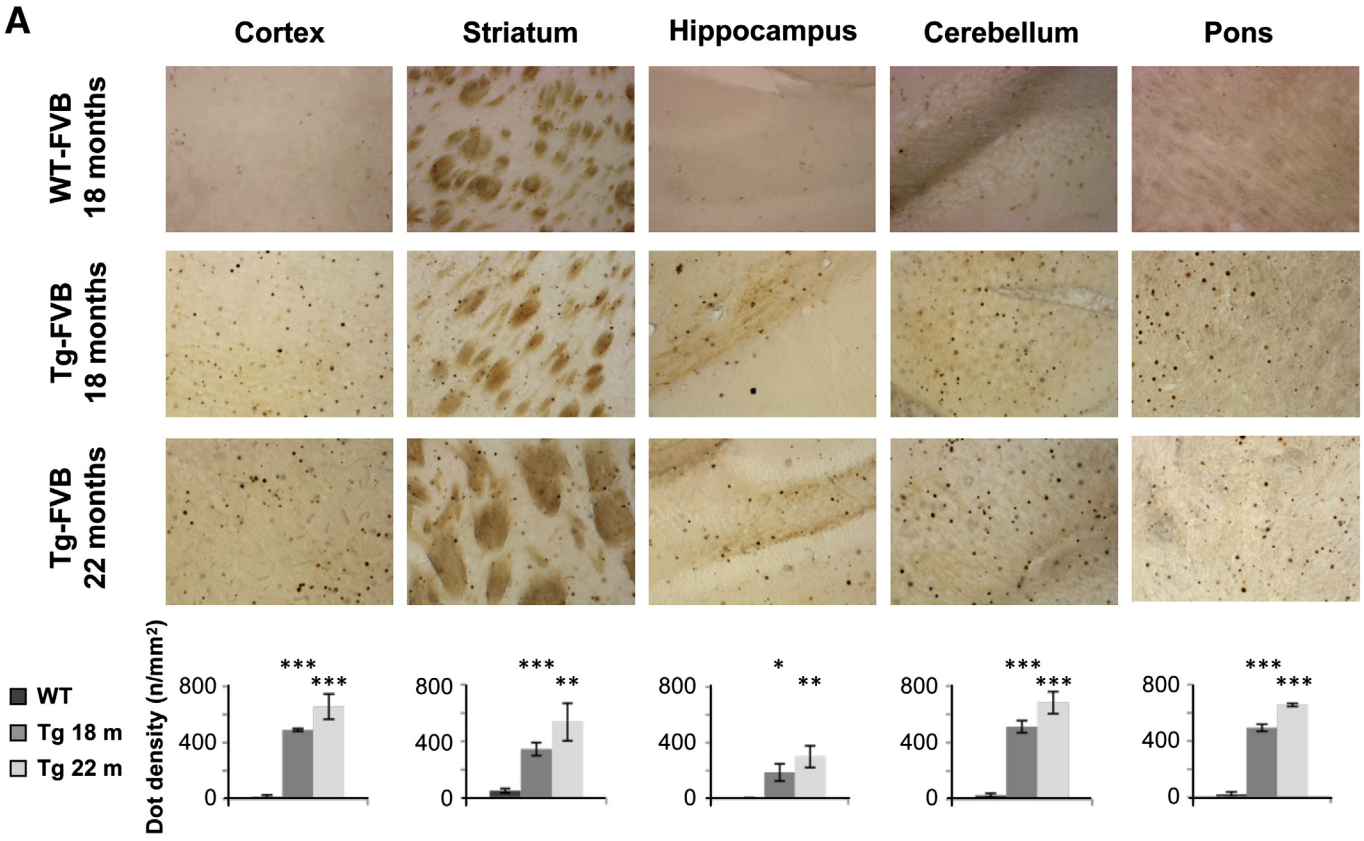

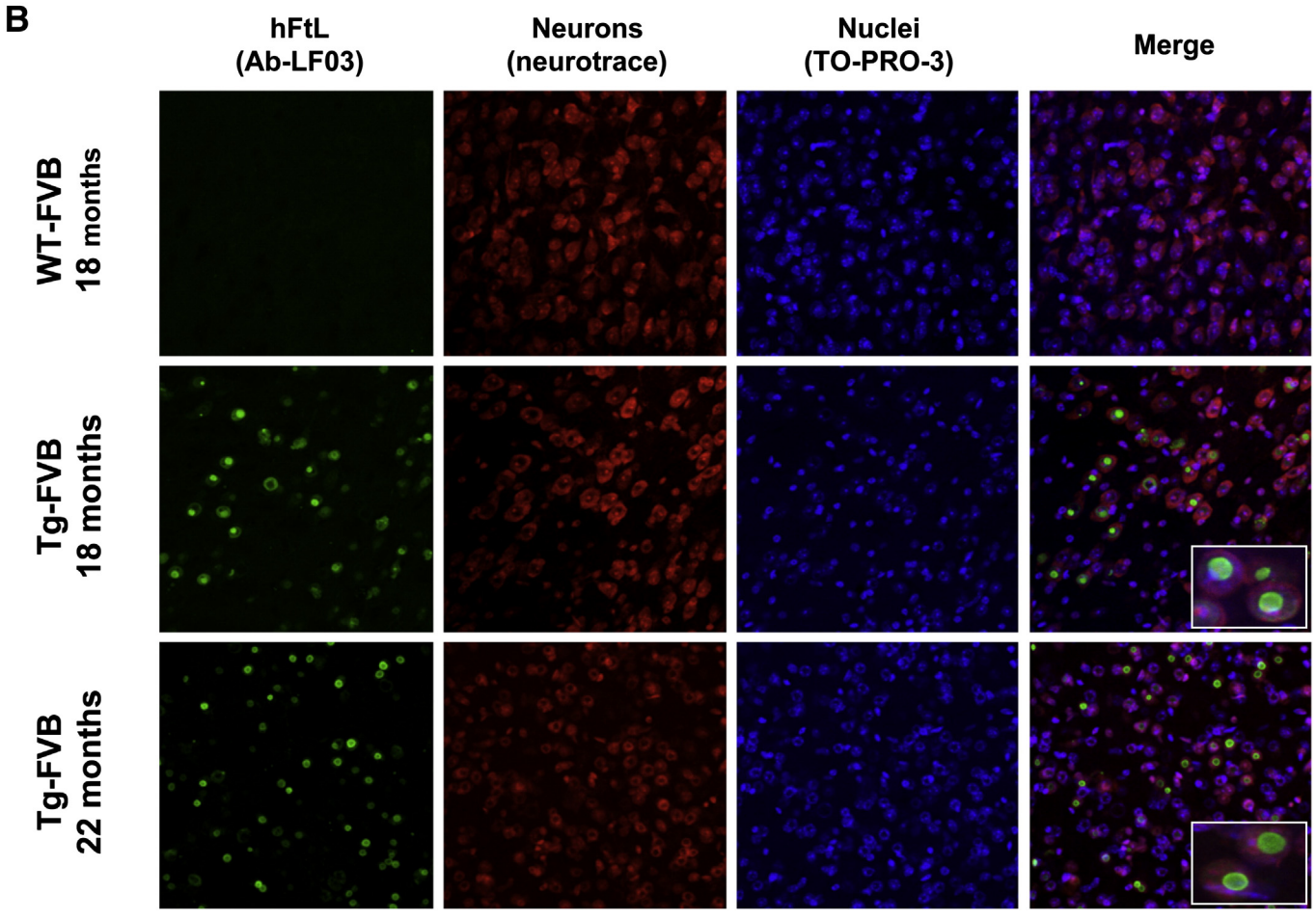

Please cite this article as: Maccarinelli, F., et al., A novel neuroferritinopathy mouse model (*FTL* 498InsTC) shows progressive brain iron..., Neurobiol. Dis. (2014), http://dx.doi.org/10.1016/j.nbd.2014.10.023

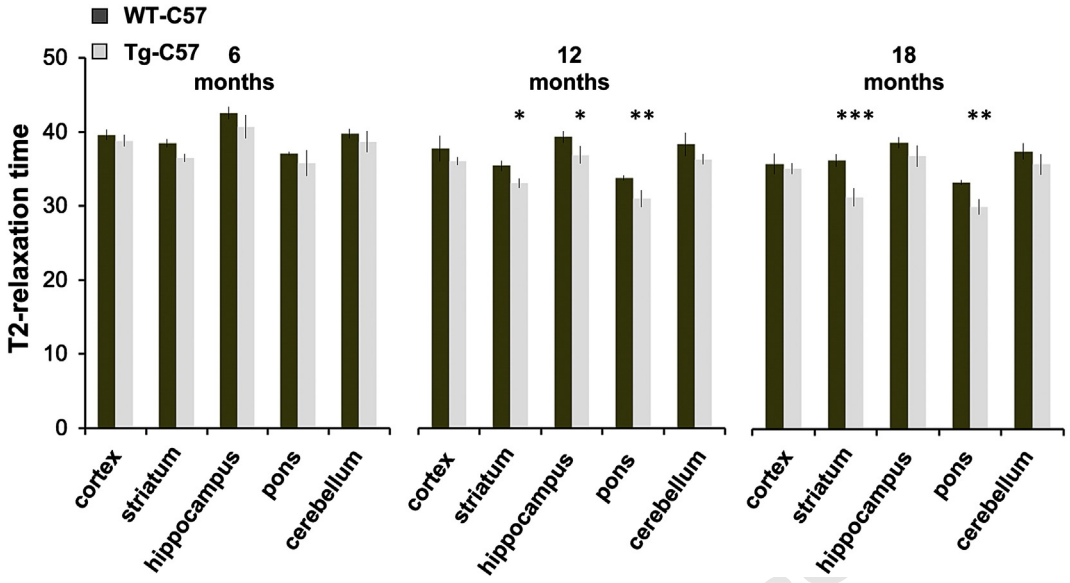

Fig. 5. MRI reveals that brain iron accumulation increases during aging. *In vivo* T2 relaxation times of Tg- and WT- C57 mice at 6, 12 and 18 months of age measured on T2 maps. At 6 months a trend of T2 reduction was observed in the brains of Tg mice, but this reduction became significant at 12 and 18 months of age at the level of the striatum and pons (*p ≤ 0.05; **p ≤ 0.01; ***p ≤ 0.001).

Brain sections were also decorated with a monoclonal antibody for hFtL, Neurotrace as a neuronal marker and TO-PRO-3 for nuclei. The images show the presence of aggregates of human ferritin inside neurons in Tg-FVB mice at both 18 and 22 months (Fig. 4B).

Transgenic mice in the C57BL/6 J background show lower accumulation of iron and ferritin but maintain oxidative damage

To perform behavioral analysis, we backcrossed transgenic FVB strain with C57BL/6J (C57) mice for >6 generations (see Material and methods) to obtain an incipient congenic strain where the mutant *FTL* is stably expressed. The C57 strain is widely used in behavioral studies to investigate motor and higher brain functions. We initially found that the transgene ferritin was expressed at detectable level in the brain of the 12-month-old Tg-C57 mice (n = 4) (Fig. 1S, C), but, surprisingly, its accumulation was much lower than that found in the FVB strain with the same transgene (Fig. 2A upper panel). This occurred at both the transcript (not shown) and the protein level (~90% and ~93% decrease, respectively) compared to Tg-FVB brains. MRI was performed *in vivo* and no hypointense spots could be observed in SWI images of the Tg-C57 brains (not shown). However, MRI T2 maps showed a decrease in T2 relaxation times and an increase in the R2 in the brains of older transgenic mice, suggestive of diffuse neuronal iron deposition: a significant T2 reduction was measured in striatum and pons of 12 and 18-month-old mice compared to age matched controls (Fig. 5, *p ≤ 0.05; **p ≤ 0.01; ***p. ≤ 0.001). Of note, the serum endogenous ferritin levels halved in transgenic mice (from 775 ± 160 *vs* 351 ± 139; n = 4), in a way similar to what observed in neuroferritinopathy patients (McNeill et al., 2008). We then evaluated signs of increased oxidative damage. We compared brain tissues from Tg-C57 with those of WT-C57 (n = 4 + 4). We observed higher levels of oxidized proteins (OxyBlot; **p ≤ 0.001, Fig. 6A); higher levels of protein ubiquitination (immunoblotting; *p ≤ 0.05, Fig. 6B); higher lipidic peroxidation (oxy-MDA, *p ≤ 0.05, Fig. 6C) in Tg-C57 mice respect to the WT-C57. Furthermore, the evaluation of 8-OHdG resulted in higher levels of DNA oxidation (1,68 fold, *p ≤ 0.05) respect to the control mice (not shown). The altered oxidative status was also confirmed by a 1.5-fold increase (*p ≤ 0.05) in Tg-C57 mice of the expression of catalase, one of the early defense response to altered oxidative conditions (Fig. 6D).

Primary cultures of hippocampal neurons from Tg mice show increased susceptibility to oxidative stress

Based on the correlation of iron accumulation and oxidative stress observed in Tg-FVB and Tg-C57 brains, hippocampal cultures were obtained from both WT- and Tg-C57 mice. These preparations were subjected to different oxidative stress conditions to mimic, in a very short period of time, what it might occur to neurons during their lifespan. In particular, the susceptibility of neurons to the oxidative insults was evaluated in conditions of chronic iron overload (100 μM ferric iron, administered as ferric ammonium citrate, for 24 h) and/or after acute exposure to hydrogen peroxide (300 μM, added immediately before the experiment). The kinetic analysis of cell death was performed by high throughput microscopy (Pelizzoni et al., 2011), an approach that allowed to partially overcome the high variability of the measurements, largely due to the fact that in the neuronal preparations several hippocampi from littermates with mixed genotype were pooled due to technical restrictions. For all oxidative conditions, a toxic effect over time is demonstrated by the increasing percentage of Sytox-positive nuclei (a marker of cell death); however, this effect was clearly higher in

Q1 **Fig. 4.** Ferritin and iron accumulation in section of the brain of FVB mutated mice. A DAB-enhanced Prussian Blue staining of brains of 18 and 22 month-old controls and transgenic FVB mice. The iron accumulation is documented by brown dots. The number of these dots was quantified, revealing a significant increase in iron deposits in Tg mice of 18 and 22 months of age (*p ≤ 0.05; **p ≤ 0.01; ***p ≤ 0.001). B Immunofluorescence analyses of the same brains performed with anti hFtL (LF03 green) antibody, Neurotrace (neuronal staining, red) and TO-PRO-3 (nuclear marker, blue). In Tg mice an increase in L-ferritin positivity with respect to control mice was detected indicating an accumulation of protein aggregates inside neurons. Higher magnifications are shown in the two inserts.

Please cite this article as: Maccarinelli, F., et al., A novel neuroferritinopathy mouse model (*FTL* 498InsTC) shows progressive brain iron..., Neurobiol. Dis. (2014), http://dx.doi.org/10.1016/j.nbd.2014.10.023

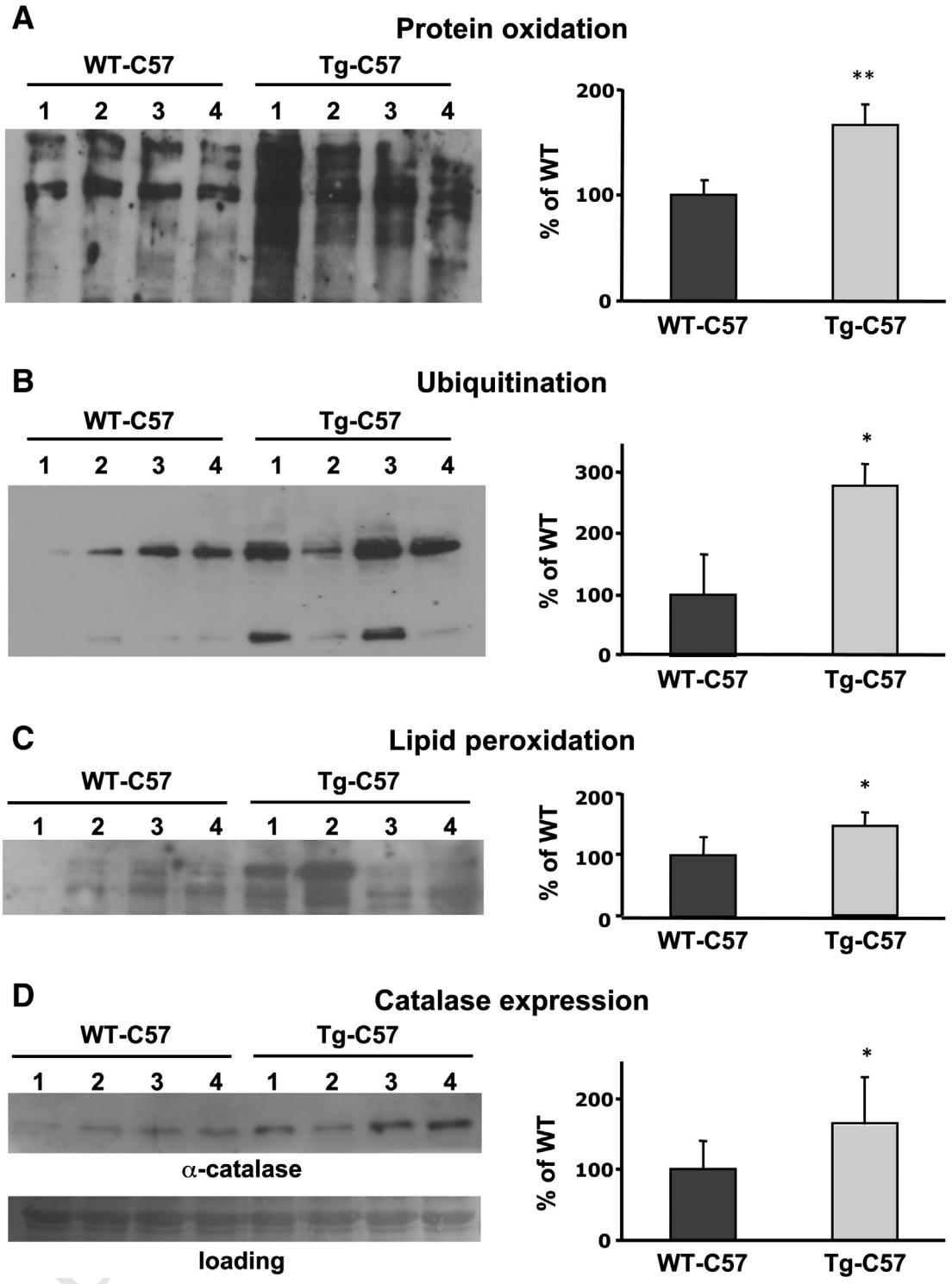

Fig. 6. Tg-C57 brains maintain oxidative damage. Soluble fractions of brains of WT-C57 and Tg-C57 12-months-old were analyzed on 12% SDS-PAGE, subjected to immunoblotting. A The oxidized proteins (1 μg) were detected by treating with DNPH and blotted with anti-DNP antibody. B After electrophoretic analysis, 20 μg of brain homogenates were blotted with an anti-ubiquitin antibody. C 10 μg of soluble proteins of homogenate were tested for MDA–protein adducts measured by the OxiSelect MDA immunoblot Kit. D 25 μg of total soluble proteins was blotted and incubated with an anti-catalase antibody. Immunoblotting shows one representative of three independent experiments. Quantification of band area was performed by densitometry and expressed as % of WT; results are the mean of three independent experiments.

the neurons from Tg-C57 than in those from WT-C57 matings (Fig. 7A). The statistical analysis of the number of dead cells at the end of the experiments (90 min) shows a significant difference between the two populations, analyzed after both 7 and 14 days in culture (Fig. 7B), indicating an increased susceptibility for oxidative damage of neural populations enriched for mutant FtL in respect with pure WT neurons.

Tg-C57 mice show iron and lipofuscin accumulation

Brain tissues were investigated at the ultrastructural level for possible histologic hallmarks of neurodegeneration as early signs of a developing neuroferritinopathy; the presence of these signs is essential to assess the suitability of our animal model to investigate early

Please cite this article as: Maccarinelli, F., et al., A novel neuroferritinopathy mouse model (*FTL* 498InsTC) shows progressive brain iron..., Neurobiol. Dis. (2014), http://dx.doi.org/10.1016/j.nbd.2014.10.023

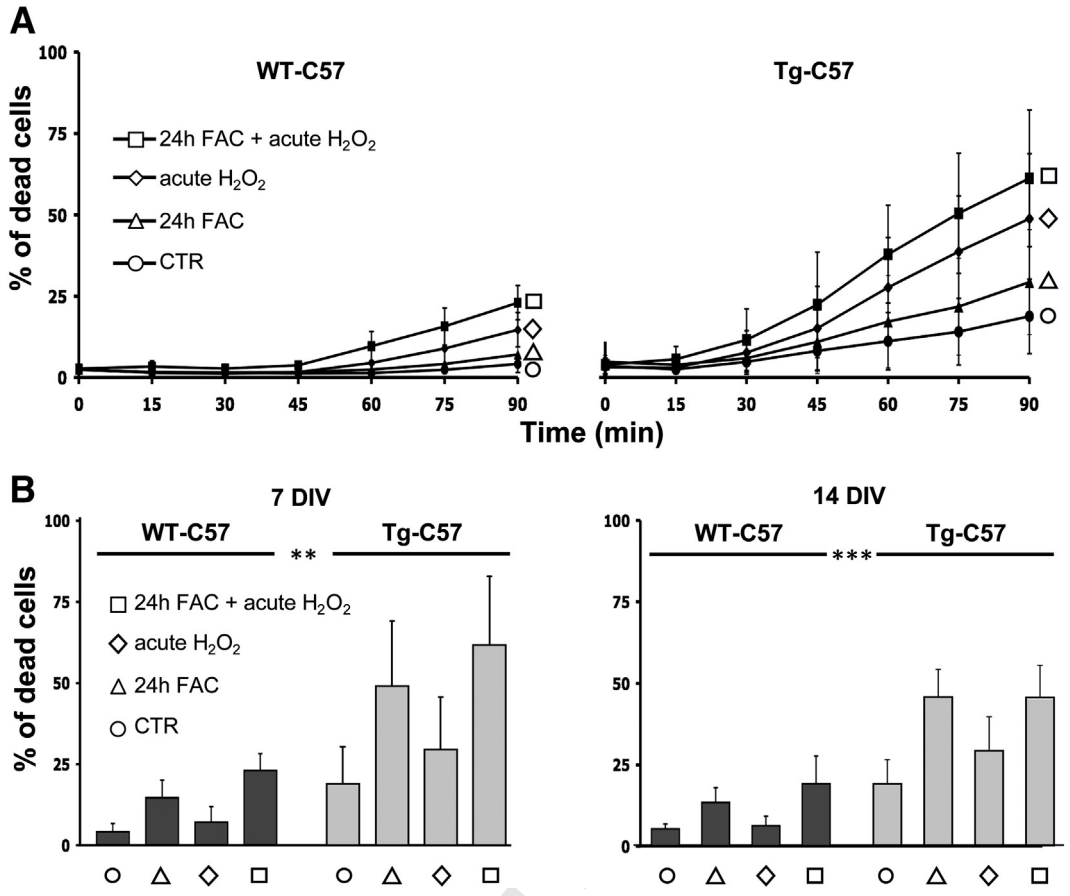

Fig. 7. Primary hypocampal neurons from Tg-C57 mice show increase susceptibility to oxidative stress. A Kinetic data were recorded from 3 independent experiments for each genotype, in duplicate (1000 cells per condition). Chronic iron overload was performed by 24 hour treatments with 100 μM ferric ammonium citrate (24 h FAC), while hydrogen peroxide (H_2O_2, 300 μM) was administered immediately before starting the image acquisition. The bars represent the standard errors. B The percentage of cell death was analyzed under the indicated conditions at the end point of the kinetics. Statistical significance was tested using two-way ANOVA followed by Bonferroni post hoc test. $^{**}p \leq 0.01$; $^{***}p \leq 0.001$. DIV = days *in vitro*.

pathogenetic events of the disease. The presence of relatively small, membrane bounded and vacuolated, osmophilic bodies was detected in 12 month-old mice (Fig. 8A). However, they were more abundant in Tg-C57 than in WT-C57 mice (about one order of magnitude in the average). Moreover, while their regional distribution was homogeneous in WT brains, a higher density (about 3 folds) was observed in the striatum of Tg mice. The ultrastructural localization of these osmophilic bodies was cytoplasmatic with no evidence of their presence in either the nucleus or extracellularly. They were typically composed of a granular matrix, with irregularly distributed dark-black dots, and a vesicle with a clear inner matrix.

The presence of these osmophilic bodies has long been reported in anatomical and histochemical studies and referred to as lipofuscin granules, i.e. pigment granules containing lipid residues of the lysosomal digestion and metals. Accordingly, we employed electron spectroscopic imaging (ESI), a technique which allows high resolution elemental analysis of thin sections, to look for the presence of iron. In Fig. 8B, a pair of pictures are presented where the image to the left illustrates the ultrastructural organization at 240 eV (i.e., below the carbon K-edge), and that to the right shows the same image with superimposed the ESI iron distribution (coded from dark to light red, low to high values, respectively). The ESI analysis of brain tissue revealed high iron signals within the granular matrix and the dense dots. No comparable signals where observed in other subcellular compartments.

To further confirm the presence of lipofuscin in these osmophilic bodies, we studied their autofluorescence properties. The emission of fluorescence from putative lipofuscin granules was excited at three wavelengths (458, 514 and 543 nm). With increasing excitation wavelength, the emission maximum shifted towards longer wavelengths and spectral width (Fig. 8C) was decreased as previously reported for lipofuscin accumulations in the retina (Sparrow, 2010).

Tg-C57 mice develop a motor coordination impairment with aging

As a final characterization of our model of neuroferritinopathy, we evaluated the motor coordination by using the natural fear of falling response. The rotarod test revealed a significant effect of trials in young (main effect of trial $F(2,52) = 16.884$, $^{***}p \leq 0.0001$), adult (main effect of trial $F(2,108) = 36.772$, $^{***}p \leq 0.0001$) and old (main effect of trial $F(2,34) = 4.730$, $^{*}p \leq 0.05$) mice showing a typical training curve. Analysis of motor performance of transgenic mice on the rotating rod revealed no difference in the latency to fall either at the earliest age tested, (2 months) (no main effect of genotype $F(1,26) = 1.803$, $p \leq 0.1909$) or in the adult group (no main effect of genotype $F(1,54) = 0.406$, $p \leq 0.5267$). Regardless of gender, at 18 months of age Tg-C57 mice fell earlier from the apparatus compared to wild-type subjects (main effect of genotype $F(1,17) = 15.317$, $^{**}p \leq 0.001$ and interaction between genotype and trials $F(2,34) = 3.255$, $^{*}p \leq 0.05$), an effect suggesting impaired motor coordination building up with age (Fig. 8D). Interestingly, female Tg-C57 subjects in trial 3 performed better than males, although not significantly, indicating a less penetrant phenotype in females at old age (interaction among trial, genotype and gender $F(1,34) = 2.934$, $p \leq 0.0668$).

Discussion

Alteration of cellular oxidative status is a main determinant in neurodegeneration (Rouault, 2013), and iron excess is one of the principal

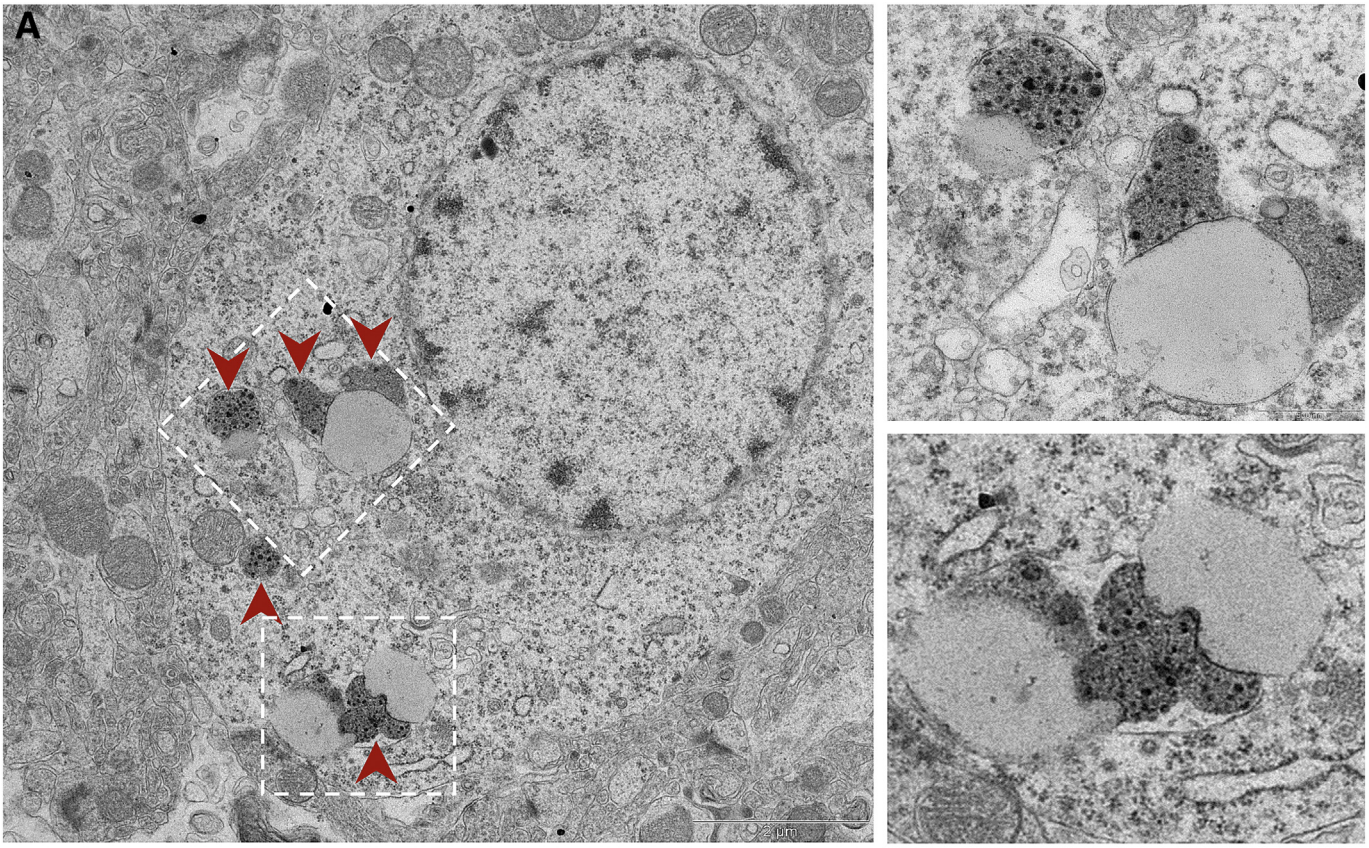

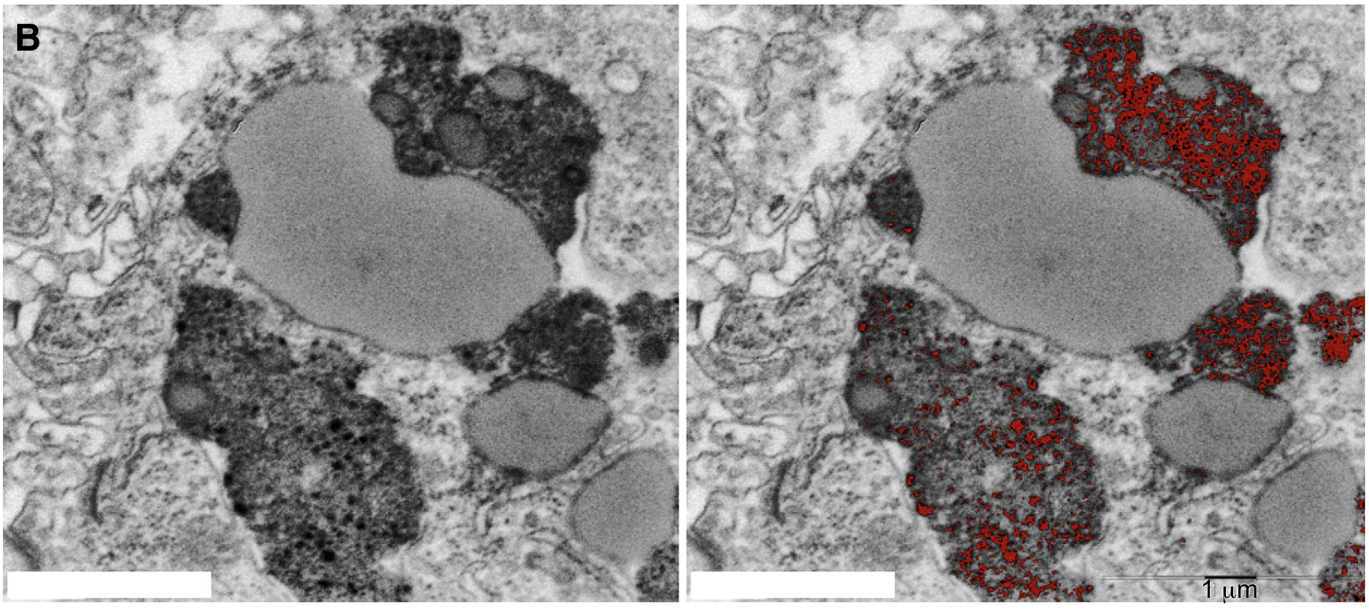

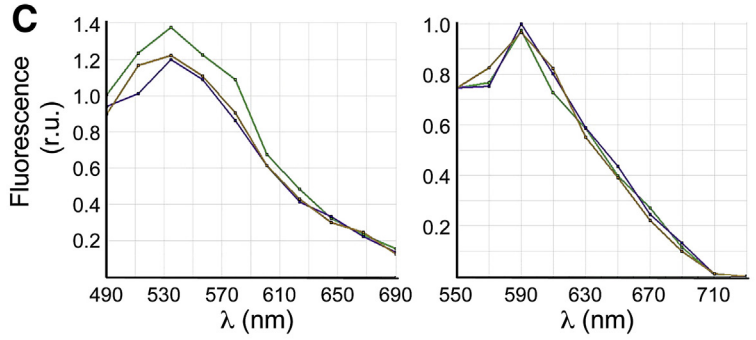

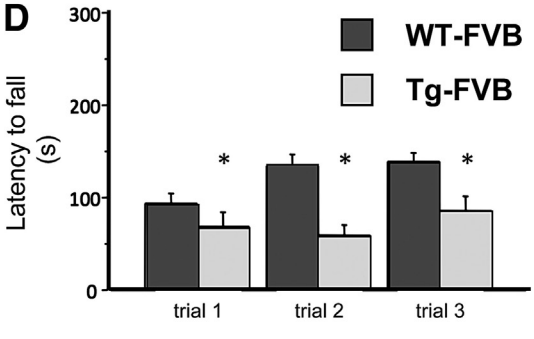

Please cite this article as: Maccarinelli, F., et al., A novel neuroferritinopathy mouse model (*FTL* 498InsTC) shows progressive brain iron..., Neurobiol. Dis. (2014), http://dx.doi.org/10.1016/j.nbd.2014.10.023

causes of oxidative stress (Halliwell and Gutteridge, 1992). However, the interplay among iron, oxidative damage and neurodegeneration is not fully understood. Neuroferritinopathy constitutes an interesting pathogenic model to study the interplay among all these factors. Previous studies on patients' autoptic samples (Curtis et al., 2001; Baraibar et al., 2012) as well as on animal (Vidal et al., 2008; Barbeito et al., 2009) and cellular models (Barbeito et al., 2010; Cozzi et al., 2006, 2010) have suggested a few elements as key factors involved in the etiopathogenesis of the disease: i) alteration of iron metabolism, ii) increased oxidative stress and iii) formation of aggregates of iron and ferritin. To prove that these events are interrelated and that their concomitant action leads to neuronal death, we generated two new transgenic mouse models overexpressing the 498–499InsTC human ferritin mutant, under the PGK promoter, in FVB and in C57 strains. This latter mouse model is analogous to that described by Vidal (Vidal et al., 2008), but the transgene is under the PGK promoter instead of the Prion protein one used by Vidal (Vidal et al., 2008). Notably, the prion protein promoter has a much more neuron-selective and powerful expression than the PGK promoter (Borchelt et al., 1996). Hence our C57 mouse model, characterized by a more attenuated and, thus, a more physiological expression of the mutant *FTL* gene, might better recapitulate the human disease.

Although the transgene was expressed in all tissues tested, we focused our analysis on the brain, the organ in which neuroferritinopathy is pathogenic. The expression of the transgene product progressively increased with age and was paralleled by an elevation of the endogenous ferritins and down-regulation of TfR1. This response is consistent with an elevation of free cytosolic iron, a condition that modulate, in an opposite way, ferritins and TfR1 translation, via the IRE/IRPs machinery. Therefore these data strongly suggest that the increase in ferritin levels leads to a decrease in iron buffering capacity and not in an elevation, as it would be expected in conditions of overexpression of the native protein (Cozzi et al., 2000).

Based on this premise, we hypothesized that the biophysical properties of the transgenic ferritin in storing iron were altered. To address this point, we investigated recombinant ferritins at the molecular level. A critical issue might be the composition of different subunits in the shell. As previously demonstrated *in vitro* (Luscieti et al., 2010) and as expected by the dominant transmission of the disease, a low percentage of the variant peptide is sufficient to strongly reduce the capacity of ferritin to incorporate iron. Accordingly, we produced heteropolymer ferritins characterized by a high proportion of H chains (21–22 per 24-mer) and a low proportion of the FtL WT or the $FtL_{167Sfsx26}$.

Cyclic voltammetry analysis revealed that the variant ferritin facilitates the release of iron from the shell thereby reducing the overall capacity to retain iron within the inner cavity.

The lower ability of the mutated protein to buffer iron can account for the elevation of the iron reported in patient's brain and documented by the MRI and by the presence of granules of ferritin and iron in the autoptic samples (Curtis et al., 2001; Baraibar et al., 2012). A very similar condition was observed in the brain of the aged transgenic mice, which showed hypodense areas at the MRI, typical signs of an accumulation of hemosiderin and ferritin within tissues (Robinson and Bhuta, 2011). In particular, in the FVB mutant mice, both T2 and SWI MRI sequences demonstrated the *in vivo* presence of multiple small dark hypointense areas in the basal ganglia and hippocampi highly suggestive for sites of iron accumulation. MRI T2-relaxometry is a sensitive technique for the *in vivo* assessment of brain iron content that has already been employed for iron load quantification in different neurological disorders, including PKAN, multiple sclerosis an Parkinson's disease (Zorzi et al., 2011; Khalil et al., 2009; Mondino et al., 2002) as well as in neuroferritinopahy (McNeill et al., 2008). A significant accumulation of iron within the striatum, hippocampus and pons was further confirmed, *ex vivo*, by the presence of histochemical positivity for iron. The number and size of the Fe^{3+}-positive granules increased with age, in parallel with the accumulation of the exogenous ferritin, mainly localized in neurons.

Additional information was provided by the elemental analysis at the ultrastructural level that revealed iron accumulation within the granular matrix of osmophilic bodies. These bodies were membrane bound and contained vacuolated areas with a clear inner matrix; fluorescence spectral analysis provided conclusive evidence that these granules were lipofuscin and not neuromelanin granules, although they share similar morphology (Double et al., 2008). Notably, although iron aggregates were typically localized close the nucleus, we never observed any nuclear accumulation of this ion. This is at variance with what was reported in the previous mouse model for the same mutation; a reason for this discrepancy may be related to the lower expression of the transgene in our mutant mice (Vidal et al., 2008). However, lack of elemental analysis in the article from the Vidal laboratory makes difficult to compare these morphological aspects.

All our findings point to an altered kinetics of iron uptake/release of the $FtH/FtL_{F167SfsX26}$, which are expected to result in higher availability of free iron. In turn, higher levels of cytoplasmic iron are expected to promote the Fenton reaction whose end-products are ROS. This dynamics is supported by molecular evidence *in vitro*, where the higher availability of iron around the electrodes coated with the mutated FtL protein caused, in the buffer solution, a potent increase in ROS. We substantiated this observation with conclusive evidence of increased ROS production and of oxidative damage in the brain tissue derived from our transgenic mice by dosing oxidation of proteins, lipids, and nucleic acids with a variety of techniques. Notably, primary neuronal cultures derived from our mouse model showed an increased susceptibility to iron-induced-death, thus providing strong evidence that the basal oxidative stress is coupled with a reduced antioxidant cellular defense, a condition which actively cooperates in cell damage. Along this line is the observation of an the increased presence of lipofuscine granules. In fact, lipofuscin is a well-known hallmark of aging, hence its alternate name of "age pigment", and the rate of its accumulation is reported to correlate negatively with longevity (Brunk and Terman, 2002). A number of experimental evidence have previously linked lipofuscine accumulation with oxidative stress. In particular, it has been reported that the oxidation of 26S proteasome by a variety of altered pathways (Reinheckel et al., 2000) promotes its disassembly (and consequent accumulation of polyubiquitinated proteins (Wang et al., 2010). This occurrence starts a cascade of events that ultimately leads to the formation of lipofuscin-containing aggregosomes (Hohn and Grune, 2013). Interestingly, iron has been described as an activator of lipofuscine formation and a major component of these aggregosomes (Brunk and Terman, 2002). Lipofuscine accumulates within the Q11 lysosomes where the degradation of iron-containing proteins, such as cytochromes and ferritin, leads to the release of redox-active free iron. Then, lipofuscine is able to adsorb ferrous iron thus constituting a redox-active surface that catalyzes the Fenton reaction with generation

Fig. 8. Tg-C57 mice show iron and lipofuscin accumulation and behavioral alteration. A A conventional representation of the ultrastructural organization shows osmophilic bodies (arrowheads) characterized by the presence of a granular matrix, containing irregularly distributed dark-black dots, and a vacuole with a clear inner matrix (see two blow up in the insets on the right). These bodies were typically localized close to the nucleus. B Subcellular iron map obtained by ESI. The image on the left shows the ultrastructural organization as seen at 250 eV (represented with inverted gray tone values). On the right, the same image with superimposed the net iron map represented by pseudocolors, ranging from dark red to yellow (low to high iron content). Iron appears to be concentrated within the granular matrix of the osmophilic bodies. C The autofluorescence properties of these osmophilic bodies were investigated upon excitation at two excitation wavelengths: 458 and 514 nm. With increasing excitation wavelength, the emission maximum shifted towards longer wavelengths and spectral width was decreased as previously reported for lipofuscin accumulations. D Assessment of motor function using the rotarod test. Aged Tg mice (18 months) showed poorer motor coordination compared to wild-type subjects. Results are presented as mean + S.E.M. * $p \leq 0.05$; ($n = 11$ WT, 10 Tg). Data from earlier ages showed no significant impairment in this test.

Please cite this article as: Maccarinelli, F., et al., A novel neuroferritinopathy mouse model (*FTL* 498InsTC) shows progressive brain iron..., Neurobiol. Dis. (2014), http://dx.doi.org/10.1016/j.nbd.2014.10.023

of hydroxyl radicals and amplification of the oxidative damage (Hohn and Grune, 2013). Within this framework, the concomitant overloading of the proteasome by all oxidized proteins, might favor a diversion of all ferritins, including their oxidized products, towards the aggregosomes in a self maintained circle of harmful events. The lysosome, overloaded by lipofuscine, may undergo rupture with direct cell damage by hydrolytic enzymes and indirect adverse effects of lipofuscine release into cytosol, where it may act as a catalyst for further iron precipitation by enhancing the formation of ferritin–iron aggregates (Fig. 9).

From a phenotypic point of view, our data indicate that *FTL* transgenic mice recapitulate not only some pathological signs of human neuroferritinopathy but also some initial neurological signs associated with the disease. In particular, higher accumulation of iron aggregates in the striatum, which is almost exclusively composed of GABAergic neurons, strictly correlates with the defects in motor coordination observed by the rotarod test. These defects were somewhat expected as a direct effect of a dysfunction of the basal nuclei. Furthermore, we scored a progressive worsening of the motor coordination parameters with age, with only 18-month-old Tg mice falling from the rotating rod before controls.

Conclusion

We can conclude that our transgenic neuroferritin model recapitulates some key pathological and clinical aspects of the initial phases of human neuroferritinopathy, including initial CNS pathological hallmarks and motor coordination deficits. Hence, the molecular characterization of this model provides new and relevant insights on the biochemical defects at the basis of the disease, pointing to the oxidative stress as the major molecular effector in the etiopathogenesis of neuroferritinopathy. Overall, our mutants represent a universal model for studying specific therapies aimed to counteract the adverse effects of oxidative stress in the brain, not only in NBIA disorders, but also in a vast group of disorders characterized by ROS production and neurodegenerative processes, including Parkinson and Alzheimer diseases.

Supplementary data to this article can be found online at http://dx.doi.org/10.1016/j.nbd.2014.10.023.

Acknowledgments

The authors wish to thank the San Raffaele Core Facility for Conditional Mutagenesis (CFCM), the Alembic Facility and the "Centro di Eccellenza di Risonanza Magnetica ad Alto Campo" (CERMAC), San Raffaele Scientific Institute, Milan; Dr. Ermanna Rovida for the ferritin 3D graphic models, Tamara Canu, Antonella Iadanza, Maurizio Strippoli, Michela Guaraldo, Maura Poli for experimental support; The authors gratefully acknowledge the contribution of Paolo Arosio to the project and Daniele Zacchetti, Paolo Santambrogio for helpful discussion. The financial support of Telethon-Italia (Grants no. GGP10099) is gratefully acknowledged. Futher support from PRIN 2008 (2008LM99R4, OC), PRIN 2010-11 (20108WT59Y_005, FG), and MIUR-RICERCA FINALIZZATA (PE-2011-02347716, OC). This work was carried out within the framework of the Ivascomar project (FG) of the Cluster Tecnologico Nazionale Scienze della Vita ALISEI (MIUR).

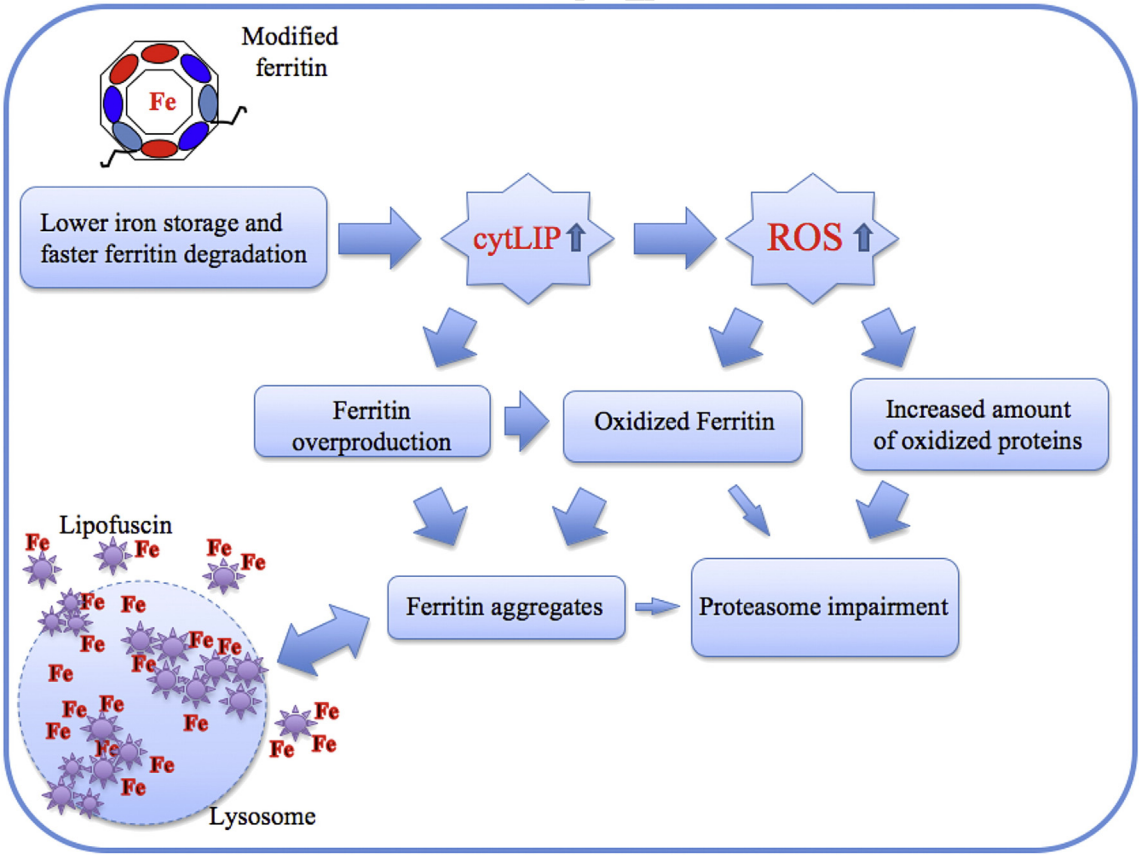

Fig. 9. Scheme of lipofuscine formation pathway. The mutation in ferritin structure induces higher levels of cytosolic free iron (cytLIP), due to its reduced ability to incorporate it, and faster degradation. Enhanced LIP promotes ferritin synthesis and ROS formation with consequent protein oxidation (including ferritin) and proteosomal impairment. Under these conditions, it is favored ferritin/iron aggregation with lysosomal degradation and lipofuscine accumulation. Following lysosome rupture may also cause lipofuscine release with further enhancing of ferritin/iron aggregation.

Please cite this article as: Maccarinelli, F., et al., A novel neuroferritinopathy mouse model (*FTL* 498InsTC) shows progressive brain iron..., Neurobiol. Dis. (2014), http://dx.doi.org/10.1016/j.nbd.2014.10.023

References

Arosio, P., Levi, S., 2010. Cytosolic and mitochondrial ferritins in the regulation of cellular iron homeostasis and oxidative damage. Biochim. Biophys. Acta 1800, 783–792.

Baraibar, M.A., Barbeito, A.G., Muhoberac, B.B., Vidal, R., 2008. Iron-mediated aggregation and a localized structural change characterize ferritin from a mutant light chain polypeptide that causes neurodegeneration. J. Biol. Chem. 283, 31679–31689.

Baraibar, M.A., Barbeito, A.G., Muhoberac, B.B., Vidal, R., 2012. A mutant light-chain ferritin that causes neurodegeneration has enhanced propensity toward oxidative damage. Free Radic. Biol. Med. 52, 1692–1697.

Barbeito, A.G., Garringer, H.J., Baraibar, M.A., Gao, X., Arredondo, M., Nunez, M.T., Smith, M.A., Ghetti, B., Vidal, R., 2009. Abnormal iron metabolism and oxidative stress in mice expressing a mutant form of the ferritin light polypeptide gene. J. Neurochem. 109, 1067–1078.

Barbeito, A.G., Levade, T., Delisle, M.B., Ghetti, B., Vidal, R., 2010. Abnormal iron metabolism in fibroblasts from a patient with the neurodegenerative disease hereditary ferritinopathy. Mol. Neurodegener. 5, 50.

Bard, A.J., Faulkner, L.R., 2001. Electrochemical Methods, Fundamentals And Applications. John Wiley & Sons, New York.

Borchelt, D.R., Davis, J., Fischer, M., Lee, M.K., Slunt, H.H., Ratovitsky, T., Regard, J., Copeland, N.G., Jenkins, N.A., Sisodia, S.S., Price, D.L., 1996. A vector for expressing foreign genes in the brains and hearts of transgenic mice. Genet. Anal. 13, 159–163.

Brooks, S.P., Dunnett, S.B., 2009. Tests to assess motor phenotype in mice: a user's guide. Nat. Rev. 10 (7), 519–529.

Brunk, U.T., Terman, A., 2002. Lipofuscin: mechanisms of age-related accumulation and influence on cell function. Free Radic. Biol. Med. 33, 611–619.

Codazzi, F., Di Cesare, A., Chiulli, N., Albanese, A., Meyer, T., Zacchetti, D., Grohovaz, F., 2006. Synergistic control of protein kinase C gamma activity by ionotropic and metabotropic glutamate receptor inputs in hippocampal neurons. J. Neurosci. 26, 3404–3411.

Cozzi, A., Corsi, B., Levi, S., Santambrogio, P., Albertini, A., Arosio, P., 2000. Overexpression of wild type and mutated human ferritin H-chain in HeLa cells: in vivo role of ferritin ferroxidase activity. J. Biol. Chem. 275, 25122–25129.

Cozzi, A., Santambrogio, P., Corsi, B., Campanella, A., Arosio, P., Levi, S., 2006. Characterization of the l-ferritin variant 460InsA responsible of a hereditary ferritinopathy disorder. Neurobiol. Dis. 23, 644–652.

Cozzi, A., Rovelli, E., Frizzale, G., Campanella, A., Amendola, M., Arosio, P., Levi, S., 2010. Oxidative stress and cell death in cells expressing L-ferritin variants causing neuroferritinopathy. Neurobiol. Dis. 37, 77–85.

Crawley, J.N., 1999. Behavioral phenotyping of transgenic and knockout mice: experimental design and evaluation of general health, sensory functions, motor abilities, and specific behavioral tests. Brain Res. 835 (1), 18–26.

Curtis, A.R., Fey, C., Morris, C.M., Bindoff, L.A., Ince, P.G., Chinnery, P.F., Coulthard, A., Jackson, M.J., Jackson, A.P., McHale, D.P., Hay, D., Barker, W.A., Markham, A.F., Bates, D., Curtis, A., Burn, J., 2001. Mutation in the gene encoding ferritin light polypeptide causes dominant adult-onset basal ganglia disease. Nat. Genet. 28, 350–354.

Deng, X., Vidal, R., Englander, E.W., 2010. Accumulation of oxidative DNA damage in brain mitochondria in mouse model of hereditary ferritinopathy. Neurosci. Lett. 479, 44–48.

Devos, D., Tchofo, P.J., Vuillaume, I., Destee, A., Batey, S., Burn, J., Chinnery, P.F., 2009. Clinical features and natural history of neuroferritinopathy caused by the 458dupA FTL mutation. Brain 132, e109. http://dx.doi.org/10.1093/brain/awn274.

Do, J., Kim, J.I., Bakes, J., Lee, K., Kaang, B.K., 2013. Functional roles of neurotransmitters and neuromodulators in the dorsal striatum. Learn. Mem. 20 (1), 21–28.

Double, K.L., Dedov, V.N., Fedorow, H., Kettle, E., Halliday, G.M., Garner, B., Brunk, U.T., 2008. The comparative biology of neuromelanin and lipofuscin in the human brain. Cell. Mol. Life Sci. 65, 1669–1682.

Dusek, P., Schneider, S.A., 2012. Neurodegeneration with brain iron accumulation. Curr. Opin. Neurol. 25, 499–506.

Follenzi, A., Ailles, L.E., Bakovic, S., Geuna, M., Naldini, L., 2000. Gene transfer by lentiviral vectors is limited by nuclear translocation and rescued by HIV-1 pol sequences. Nat. Genet. 25, 217–222.

Halliwell, B., Gutteridge, J.M., 1992. Biologically relevant metal ion-dependent hydroxyl radical generation. An update. FEBS Lett. 307, 108–112.

Hohn, A., Grune, T., 2013. Lipofuscin: formation, effects and role of macroautophagy. Redox Biol. 1, 140–144.

Khalil, M., Enzinger, C., Langkammer, C., Tscherner, M., Wallner-Blazek, M., Jehna, M., Ropele, S., Fuchs, S., Fazekas, F., 2009. Quantitative assessment of brain iron by R(2)* relaxometry in patients with clinically isolated syndrome and relapsing–remitting multiple sclerosis. Mult. Scler. 15, 1048–1054.

Kubota, A., Hida, A., Ichikawa, Y., Momose, Y., Goto, J., Igeta, Y., Hashida, H., Yoshida, K., Ikeda, S., Kanazawa, I., Tsuji, S., 2009. A novel ferritin light chain gene mutation in a Japanese family with neuroferritinopathy: description of clinical features and implications for genotype–phenotype correlations. Mov. Disord. 24, 441–445.

Levi, S., Finazzi, D., 2014. Neurodegeneration with brain iron accumulation: update on pathogenic mechanisms. Front. Pharmacol. 5, 99. http://dx.doi.org/10.3389/fphar.2014.00099.

Luscieti, S., Santambrogio, P., Langlois d'Estaintot, B., Granier, T., Cozzi, A., Poli, M., Gallois, B., Finazzi, D., Cattaneo, A., Levi, S., Arosio, P., 2010. Mutant ferritin L-chains that cause neurodegeneration act in a dominant-negative manner to reduce ferritin iron incorporation. J. Biol. Chem. 285, 11948–11957.

Maciel, P., Cruz, V.T., Constante, M., Iniesta, I., Costa, M.C., Gallati, S., Sousa, N., Sequeiros, J., Coutinho, P., Santos, M.M., 2005. Neuroferritinopathy: missense mutation in FTL causing early-onset bilateral pallidal involvement. Neurology 65, 603–605.

Mancuso, M., Davidzon, G., Kurlan, R.M., Tawil, R., Bonilla, E., Di Mauro, S., Powers, J.M., 2005. Hereditary ferritinopathy: a novel mutation, its cellular pathology, and pathogenetic insights. J. Neuropathol. Exp. Neurol. 64, 280–294.

McNeill, A., Birchall, D., Hayflick, S.J., Gregory, A., Schenk, J.F., Zimmerman, E.A., Shang, H., Miyajima, H., Chinnery, P.F., 2008. T2* and FSE MRI distinguishes four subtypes of neurodegeneration with brain iron accumulation. Neurology 70, 1614–1619.

Mondino, F., Filippi, P., Magliola, U., Duca, S., 2002. Magnetic resonance relaxometry in Parkinson's disease. Neurol. Sci. 23 (Suppl. 2), S87–S88.

Muhoberac, B.B., Vidal, R., 2013. Abnormal iron homeostasis and neurodegeneration. Front. Aging Neurosci. 5, 32.

Nishida, K., Garringer, H.J., Futamura, N., Funakawa, I., Jinnai, K., Vidal, R., Takao, M., 2014. A novel ferritin light chain mutation in neuroferritinopathy with an atypical presentation. J. Neurol. Sci. 342 (1–2), 173–177. http://dx.doi.org/10.1016/j.jns.2014.03.060.

Ohta, E., Takiyama, Y., 2012. MRI findings in neuroferritinopathy. Neurol. Res. Int. http://dx.doi.org/10.1155/2012/197438 (ID 197438).

Paylor, R., Spencer, C.M., Yuva-Paylor, L.A., Pieke-Dahl, S., 2006. The use of behavioral test batteries, II: effect of test interval. Physiol. Behav. 87, 95–102.

Pelizzoni, I., Macco, R., Morini, M.F., Zacchetti, D., Grohovaz, F., Codazzi, F., 2011. Iron handling in hippocampal neurons: activity-dependent iron entry and mitochondria-mediated neurotoxicity. Aging Cell 10, 172–183.

Pezzati, R., Bossi, M., Podini, P., Meldolesi, J., Grohovaz, F., 1997. High-resolution calcium mapping of the endoplasmic reticulum–Golgi–exocytic membrane system. Electron energy loss imaging analysis of quick frozen-freeze dried PC12 cells. Mol. Biol. Cell 8 (8), 1501–1512.

Plenz, D., Kitai, S.T., 1998. Up and down states in striatal medium spiny neurons simultaneously recorded with spontaneous activity in fast-spiking interneurons studied in cortex–striatum–substantia nigra organotypic cultures. J. Neurosci. 18 (1), 266–283.

Reinheckel, T., Ullrich, O., Sitte, N., Grune, T., 2000. Differential impairment of 20S and 26S proteasome activities in human hematopoietic K562 cells during oxidative stress. Arch. Biochem. Biophys. 377, 65–68.

Ritzert, N.L., Casella, S.S., Zapien, D.C., 2009. Electrochem. Commun. 11, 827–830.

Robinson, R.J., Bhuta, S., 2011. Susceptibility-weighted imaging of the brain: current utility and potential applications. J. Neuroimaging 21, e189–e204. http://dx.doi.org/10.1111/j.1552-6569.2010.00516.x.

Rouault, T.A., 2013. Iron metabolism in the CNS: implications for neurodegenerative diseases. Nat. Rev. Neurosci. 14, 551–564.

Sparrow, J.R., 2010. Bisretinoids of RPE lipofuscin: trigger for complement activation in age-related macular degeneration. Adv. Exp. Med. Biol. 703, 63–74.

Vidal, R., Ghetti, B., Takao, M., Brefel-Courbon, C., Uro-Coste, E., Glazier, B.S., Siani, V., Benson, M.D., Calvas, P., Miravalle, L., Rascol, O., Delisle, M.B., 2004. Intracellular ferritin accumulation in neural and extraneural tissue characterizes a neurodegenerative disease associated with a mutation in the ferritin light polypeptide gene. J. Neuropathol. Exp. Neurol. 63, 363–380.

Vidal, R., Miravalle, L., Gao, X., Barbeito, A.G., Baraibar, M.A., Hekmatyar, S.K., Widel, M., Bansal, N., Delisle, M.B., Ghetti, B., 2008. Expression of a mutant form of the ferritin light chain gene induces neurodegeneration and iron overload in transgenic mice. J. Neurosci. 28, 60–67.

Wang, X., Yen, J., Kaiser, P., Huang, L., 2010. Regulation of the 26S proteasome complex during oxidative stress. Sci. Signal. 3, ra88. http://dx.doi.org/10.1126/scisignal.2001232.

Zorzi, G., Zibordi, F., Chiapparini, L., Bertini, E., Russo, L., Piga, A., Longo, F., Garavaglia, B., Aquino, D., Savoiardo, M., Solari, A., Nardocci, N., 2011. Iron-related MRI images in patients with pantothenate kinase-associated neurodegeneration (PKAN) treated with deferiprone: results of a phase II pilot trial. Mov. Disord. 26, 1756–1759.

Please cite this article as: Maccarinelli, F., et al., A novel neuroferritinopathy mouse model (*FTL* 498InsTC) shows progressive brain iron..., Neurobiol. Dis. (2014), http://dx.doi.org/10.1016/j.nbd.2014.10.023